SPECIAL REPORT 91-16

A One-Dimensional Temperature Model for a Snow Cover

Technical Documentation for SNTHERM.89

Rachel Jordan

October 1991

For conversion of SI metric units to U.S./British customary units of measurement consult ASTM Standard E380, Metric Practice Guide, *published by the American Society for Testing and Materials, 1916 Race St., Philadelphia, Pa. 19103.*

This report is printed on paper that contains a minimum of 50% recycled material.

Special Report 91-16

U.S. Army Corps of Engineers
Cold Regions Research & Engineering Laboratory

A One-Dimensional Temperature Model for a Snow Cover

Technical Documentation for SNTHERM.89

Rachel Jordan

October 1991

Prepared for
OFFICE OF THE CHIEF OF ENGINEERS

PREFACE

This report was prepared by Rachel Jordan, Physicist, Geophysical Sciences Branch, Research Division, U.S. Army Cold Regions Research and Engineering Laboratory. Funding for this report was provided by DA Project 4A161102AT24, *Cold Regions Surface-Air Boundary Transfer Processes*, Task FS, Work Unit 010. This project was conducted for the Directorate for Research and Development of the Office of the Chief of Engineers, U.S. Army Corps of Engineers.

This report describes a working model that is still in development. Inconsistencies will be addressed in the subsequent model and the report that will accompany it. The author welcomes comments on any aspects of this model.

Computer programming support for the one-dimensional mass and energy transport model was provided by James Jones of Sparta Systems, Inc., Lexington, Massachusetts. Funding for this support was provided by the Smart Weapons Operability Enhancement program.

This document was technically reviewed by Dr. Robert E. Davis and Dr. Joyce Nagle of CRREL. The equations in the manuscript were typed by Sandra Smith of CRREL.

The author appreciates the help provided by numerous individuals who have shared information in their areas of expertise: Dr. Mary Albert, Dr. Edgar Andreas, Dr. Patrick Black, Dr. Samuel Colbeck, Dr. Robert Davis, Dr. Donald Perovich and Dr. Y.C. Yen.

CONTENTS

ILLUSTRATIONS

TABLES

NOMENCLATURE

All units are in the SI system, with the exception of pressure, which is expressed as either mb or N/m^2. One calorie converts to 4.1868 J.

a	Adjustable parameter in grain growth equation (m^2/s)
$a1$	Constant in freezing curve (K^{-1})
$a2$	Constant in freezing curve (K^{-1})
Ak	Coefficient in fluid flow equation $= \frac{\rho_\ell^2 \, g \, K_{max}}{\mu_\ell}$ ($kg/m^2 \cdot s$)
A	Element in tridiagonal matrix; also area
$\mathcal{A}$	Absorptivity in solar insolation routine
B	Element in tridiagonal matrix vector
b	Adjustable parameter in grain growth equation (K^{-1})
b_s	Constant term in linear approximation for s_e^3
c	Specific heat ($J/kg \cdot K$)
c_{air}	Specific heat of air at 0°C (1005.0) ($J/kg \cdot K$)
c_ℓ	Specific heat of water at 0°C (4217.7) ($J/kg \cdot K$)
c_{app}	Apparent specific heat, incorporating melt ($J/kg \cdot K$)
$c1$	Constant in computation of C_{kT} ($kg/m^3 \cdot K$)
$c3$	Snow densification constant
$c4$	Snow densification constant
$c5$	Snow densification constant (K^{-1})
$c6$	Snow densification constant (m^3/kg)
$c7$	Constant in fluid flow equation $\rho_\ell \frac{(1 - s_r)\,\Phi \Delta z}{\Delta t} = (kg/m^2 \cdot s)$
$c8$	Constant in computation of hemispherically emitted spectral radiation ($0.59544 \times 10^{-16}\ Wm^2$)
$c9$	Constant in computation of hemispherically emitted spectral radiation ($1.4388 \times 10^{-2}\ Km$)
C_{kT}	Variation of saturation vapor pressure with temperature relative to phase k ($N/m^2 \cdot K$)
C_E	Dimensionless bulk turbulent transfer coefficient for latent heat
C_D	Dimensionless bulk turbulent transfer coefficient for momentum (drag coefficient)
C_H	Dimensionless bulk turbulent transfer coefficient for sensible heat
C_{EN}	Dimensionless bulk turbulent transfer coefficient for latent heat under neutral stability
C_{DN}	Dimensionless bulk turbulent transfer coefficient for momentum under neutral stability
C_{HN}	Dimensionless bulk turbulent transfer coefficient for sensible heat under neutral stability
CR	Fractional compaction rate of snow cover (s^{-1})
d	Diameter of snow grain (m)
d_k	Constant in computation of solar insolation
D	Diffusion coefficient (m^2/s)
D_2	Constant in computation of solar insolation
D_e	Effective diffusion coefficient (m^2/s)
D_{es}	Effective diffusion coefficient for water vapor in snow (m^2/s)
D_{e0s}	Effective diffusion coefficient for water vapor in snow at 1000 mb and 0°C ($0.92 \times 10^{-4}\ m^2/s$)

D_{eg}	Effective diffusion coefficient for water vapor in soil (m^2/s)
D_{e0g}	Effective diffusion coefficient for water vapor in soil at 1000 mb and 0°C ($1.61 \times 10^{-5}\phi$) (m^2/s)
e	Slope elevation angle (radians)
E_{H0}	Windless exchange coefficient for sensible heat ($W/m^2 \cdot K$)
E_H	Exchange coefficient for sensible heat ($J/K \cdot m^3$)
E_{E0}	Windless exchange coefficient for latent heat ($W/m^2 \cdot mb$)
E_E	Exchange coefficient for latent heat ($J/mb \cdot m^3$ or Pa/mb)
fallrate	Meters of hourly accumulation of bulk precipitation (m/hr)
f_ℓ	Mass liquid-water fraction (γ_l/γ_w)
$\hat{f}_\ell$	Portion of f_ℓ that is independent of water content
$f_{\ell p}$	Mass liquid-water fraction of precipitation
f_{rh}	Fractional humidity within medium relative to saturated state (0.0–1.0)
F	Slope of freezing curve
$\bar{\hat{F}}$	Temporal average of F over temperature for the current water content
g	Acceleration due to gravity ($9.80\ m/s^2$)
$\mathbf{g}$	Gravitational vector (positive downwards) (m/s^2)
$g1$	Grain growth parameter (m^4/kg)
$g2$	Grain growth parameter (m^2/s)
g_k	Term in melt-zone switch (K)
g_v	Coefficient in melt-zone switch (Km^3/kg)
h	Specific enthalpy (J/kg)
H	Enthalpy adjustment factor
ioffset	Nodal offset between bottom of grid and bottom of flow zone
I	Energy flux (W/m^2)
$I_{emit}(\lambda)$	Intensity of hemispherically emitted spectral radiation (W/m^3)
I_{emit}	Intensity of hemispherically emitted all-wave radiation (W/m^2)
I_{top}	Energy flux across air interface (W/m^2)
I'_{top}	Energy flux across air interface, excluding solar radiation (W/m^2)
$I'_{top,v}$	Portion of I'_{top} that varies with temperature (W/m^2)
$I'_{top,k}$	Portion of I'_{top} not varying with temperature (W/m^2)
I_{sen}	Sensible heat flux across air interface (W/m^2)
I_{conv}	Convective heat flux across air interface (W/m^2)
$I_{ir}\downarrow$	Downwelling long-wave radiation flux (W/m^2)
$I_{ir}\uparrow$	Upwelling long-wave radiation flux (W/m^2)
I_{lat}	Latent heat flux across air interface (W/m^2)
$I_{ir,clear}\downarrow$	Downwelling long-wave radiation flux under clear skies (W/m^2)
I_s	Solar or short-wave radiation flux, net of downwelling and upwelling components (W/m^2)
$I_s\downarrow$	Downwelling short-wave radiation flux (W/m^2)
$I_s\uparrow$	Upwelling short-wave radiation flux (W/m^2)
$I_{s,direct}\downarrow$	Downwelling direct short-wave radiation flux (W/m^2)
$I_{s,diffuse}\downarrow$	Downwelling diffuse short-wave radiation flux (W/m^2)
$I_{s,slope}\downarrow$	Downwelling short-wave radiation flux (W/m^2) adjusted for incidence on sloped surface

I_{s00}	Solar insolation at top of atmosphere (W/m^2)
I_{top}	Surface energy balance at air interface (W/m^2)
$\mathbf{I}_R$	Radiation flux vector, net of downwelling and upwelling components (W/m^2)
j	Nodal or volume element index
j'	Nodal or volume element index relative to flow zone
j''	Nodal or volume element index for atmosphere relative to air/ground interface
J	Generalized flux
$\mathbf{J}$	Generalized flux vector, positive upwards
J^*	Flux, which may be either convective or diffusive
J_p	Plasticity index (fraction of water)
k	Index for constituents
k	von Karman constant (0.40)
k_t	Thermal conductivity ($W/K \cdot m$)
k_e	Effective thermal conductivity, including effects of vapor diffusion ($W/K \cdot m$)
$\hat{k}_e$	Coefficient on T for heat conduction at control volume interface ($W/K \cdot m^2$)
K_ℓ	Hydraulic permeability (m^2)
K_{max}	Saturation or maximum permeability (m^2)
$L_{\ell i}$	Latent heat of fusion for ice (3.335×10^5 J/kg) (Mellor 1977)
L_{vi}	Latent heat of sublimation for ice (2.838×10^6 J/kg at 273.15 K) (Mellor 1977)
$L_{v\ell}$	Latent heat of evaporation for water (2.505×10^6 J/kg at 273.15 K)
m_s	Coefficient in linear approximation for s_e^3
$M_{\ell i}$	Rate of melt ($kg/m^3 \cdot s$)
M_{vi}	Rate of sublimation ($kg/m^3 \cdot s$)
$M_{v\ell}$	Rate of evaporation ($kg/m^3 \cdot s$)
M	Melt term in fluid flow equation = $\left[\overline{M_{\ell i}\Delta z}\left(1 - \frac{\rho_\ell}{\rho_i}\overline{s}\right) - \rho_\ell \overline{s\,\Delta z\,CR}\right]$ ($kg/m^2 \cdot s$)
n	Index of top node or volume element
n'	Index of top node or volume element in flow region
N	Index of top node or volume element in atmosphere
p_{jk}	Differential pressure between phase j and k (mb or N/m^2)
P	Pressure (mb or N/m^2)
P_a, P_{air}	Atmospheric or air pressure (mb)
$P_{a\ell}$	Capillary pressure (mb or N/m^2)
P_ℓ	Pressure in liquid water (mb or N/m^2)
P_{melt}	Melt function (kg/m^3)
Pr_N	Turbulent Prandtl number at neutral stability
P_s	Snow load pressure or overburden (N/m^2)
$P_{v,\,air}$	Water vapor pressure in air (mb)
$P_{v0,\,sat}$	Saturation water vapor pressure at T = 0°C (mb)
$P_{vk,\,sat}$	Saturation water vapor pressure with respect to phase k (mb)
Q_{net}	Past net heat fluxes (W/m^2)
Q_s	Stored heat coefficient ($W/m^2 \cdot K$)
Q_{solar}	Elemental absorbed solar heat (W/m^2)
R_w	Gas constant for water vapor (461.296 $J/kg \cdot K$)

Ri	Bulk Richardson number
$\mathcal{R}$	Reflectivity in solar insolation routine
s	Liquid water saturation (fraction of voids filled by liquid water) (m^3/m^3)
s_r	Irreducible or residual liquid water saturation (m^3/m^3)
$\tilde{s}_e$	Steady-state effective liquid water saturation (m^3/m^3)
s_0	Antecedent liquid water saturation (m^3/m^3)
s_e	Effective liquid water saturation
$s_{e,\,est}$	Estimate of s_e obtained from solution to cubic equation
$\mathcal{S}$	Ratio of average diffuse radiance from the solar and antisolar quadraspheres
S	Source density or internal production term
$\mathbf{S}$	Surface vector (m^2)
Sc_N	Turbulent Schmidt number at neutral stability
T	Temperature (K)
T_L	Lower temperature limit of melt zone (K)
T_H	Upper temperature limit of melt zone (K)
T_D	Depression temperature, 273.15 – T (K)
T_{error}	Effective temperature error (K)
$\mathcal{T}$	Apparent transmissivity in solar insolation routine, which includes forward scattered component
$\mathcal{T}d$	Transmissivity in solar insolation routine
U	Mass flux ($kg/m^2 \cdot s$)
$\mathbf{U}$	Mass flux vector, positive upwards ($kg/m^2 \cdot s$)
$\mathbf{U}^*$	Mass flux vector, which may be either convective or diffusive ($kg/m^2 \cdot s$)
$U_{\ell,\,net}$	Net mass liquid water flux, averaged over past and current time steps ($kg/m^2 \cdot s$)
v_k	Seepage velocity (m/s)
$\mathbf{v}_k$	Seepage velocity vector, positive upwards (m/s)
V	Volume (m^3)
w	Wind velocity (m/s)
$\mathbf{X}$	General unknown in linear equation matrix
z	Distance of nodal midpoint from snow/ground interface (m)
z_0	Roughness length (m)
Z	Thickness of snow cover or distance of snow surface from ground interface (m)
Z'_W	Reference height above the surface for wind speed measurement (m)
Z'_T	Reference height above the surface for temperature measurement (m)
Z'_Q	Reference height above the surface for relative humidity measurement (m)
α	Albedo
α_{top}	Albedo of upper layer
β_∞	Bulk or asymptotic extinction coefficient
β_{nir}	Extinction coefficient for near-IR radiation
β_{vis}	Extinction coefficient for visible radiation
γ	Bulk density (mass/total volume) (kg/m^3)
$\delta_{k'k}$	Kronecker delta
Δz	Thickness of volume element (m)
Δt	Time step (s)
Δt_{min}	Minimum time step (s)

Δz_{min}	Thickness of thinnest volume element (m)
ΔV	Control volume, $A\Delta z$ (m^3)
$\Delta\phi_{az}$	Relative azimuthal angle of slope relative to that of sun minus π (radians)
ε	Emissivity
ε	Exponent on s_e for permeability function
ε_{air}	Clear-air all-wave bulk emissivity of atmosphere
ε'_{air}	Clear-air all-wave bulk emissivity of atmosphere with Wachtmann correction
η	Viscosity coefficient ($N \cdot s/m^2$)
η_0	Viscosity coefficient at T = 0°C and $\gamma_s = 0.0$ ($N \cdot s/m^2$)
θ_k	Fractional volume (m^3/m^3)
θ_z	Solar zenith angle (radians)
λ	Wavelength (m)
μ_ℓ	Dynamic viscosity of water at 0°C (1.787×10^{-3} $N \cdot s/m^2$)
ρ_k	Intrinsic density (kg/m^3)
ρ_{air}	Density of air at 0°C and 1000 mb (1.276 kg/m^3)
ρ_i	Intrinsic density of ice (0.917×10^3 kg/m^3)
ρ_ℓ	Intrinsic density of water (1.00×10^3 kg/m^3)
ρ_s	Density of snow, including liquid water (kg/m^3)
$\rho_{vk,\,sat}$	Equilibrium water vapor density with respect to phase k (kg/m^3)
σ	Stefan–Boltzmann constant (5.669×10^{-8} $W/m^2 \cdot K^4$) (Siegal and Howell 1972, p. 738)
ϕ	Porosity
ϕ_{asp}	Aspect angle of slope measured clockwise from north (radians)
ϕ_{sd}	Solid porosity (volume between the solids/total volume)
$\varnothing_M$	Stability function for the transfer of momentum
$\varnothing_E$	Stability function for the transfer of water vapor
$\varnothing_H$	Stability function for the transfer of heat
χ	General physical quantity
Ω	General quantity in conservation equations

Subscripts

a, air	Air
i	Ice
k	Generalized coefficient for constituent
ℓ	Liquid water
d	Dry soil constituent
s	Snow
sat	Saturated state
sd	Solid
t	Total media, snow or soil
v	Water vapor
vk, sat	Saturated vapor state relative to phase *k*
w	Combined liquid and solid water phases
p	Precipitation
E	Transfer of water vapor
H	Transfer of heat
M	Transfer of momentum
N	Neutral stability

A One-Dimensional Temperature Model For a Snow Cover
Technical Documentation for SNTHERM.89

RACHEL JORDAN

INTRODUCTION

General description of model

This report describes a one-dimensional mass and energy balance model, SNTHERM.89, for predicting temperature profiles within strata of snow and frozen soil. The model is intended for seasonal snow covers and addresses conditions found throughout the winter, from initial ground freezing in the fall to snow ablation in the spring. It is comprehensive in scope, being adaptable to a full range of meteorological conditions such as snowfall, rainfall, freeze–thaw cycles and transitions between bare and snow-covered ground. Although surface temperature prediction is the primary objective, transport of liquid water and water vapor are included as required components in the heat balance equation. Snow accumulation, ablation, densification and metamorphosis are addressed in the model, as well as their impact on the optical and thermal properties of the snow cover. The water-infiltration algorithm assumes gravitational flow and is coupled to the equilibrium temperature in frozen strata through thermodynamically derived freezing curves. It does not include the effects of capillary pressure, which are required for an accurate representation of water flow in soil. Water flow in soil is therefore discounted, and water is artificially drained from the system when infiltration reaches the snow/ground interface. The model is primarily intended for low-level water flow, and while it will handle spring runoff conditions, it will not do so as efficiently as hydrological models developed for that purpose.

A numerical solution is obtained by subdividing snow and soil layers into horizontally infinite control volumes, each of which is then subject to the governing equations for heat and mass balance. As a spatial discretization procedure, the control-volume approach of Patankar (1980) is adopted, which is similar in implementation to a finite-difference scheme. A Crank–Nicolson method is used for discretizing the time domain, which gives equal weights to past and current time periods. The diffusive and convective components of the heat and mass fluxes are numerically approximated with central-difference and upwind schemes, respectively. Governing sets of equations are linearized with respect to the unknown variables and solved by the tridiagonal-matrix algorithm. The model contains an adaptive time-step procedure that automatically adjusts between maximum and minimum values (typically between 900 and 5 s) to achieve the desired accuracy of the solution. This approach is efficient in terms of computer time, since in most instances quarter-hourly time steps are sufficient, and smaller steps, associated primarily with melt and water flow, are implemented only as needed. The

overall structure of the model is very flexible, permitting an unlimited number of nodal subdivisions and material types or layers.

The governing equations are subject to meteorologically determined boundary conditions at the air interface. Surface fluxes are computed from user-supplied meteorological observations of air temperature, dew point temperature, wind speed, precipitation and, if available, measured values of solar and incoming infrared radiation. In lieu of measurements the model provides estimates of radiation through routines that take into account solar aspect, cloud conditions, albedo and inclination of the surface (Shapiro 1987). In addition, any of the meteorological values can be estimated by user-supplied algebraic functions. The model is initialized with profiles of temperature and water content for the various strata, the accuracy of which determines the time required for the simulation to equilibrate after initiation of the computer run. Physical characteristics for the selected strata are either entered by the user or are supplied from internal data bases, currently provided for snow, sand and clay.

Background

The original objective for the one-dimensional snow model was to predict the temperature difference ΔT between the surfaces of tank tracks and undisturbed snow. The earliest version (Jordan et al. 1986) was restricted to homogeneous dry snow and permitted only three nodal subdivisions of the snow cover. Even in this simplified state, comparison of model predictions with field observations indicated promise for the approach. An improved and expanded version, SNTHERM.87, incorporated phase change, permitted vertical inhomogeneity in snow cover characteristics, and relaxed the restriction on the number of nodes. Field-test verification over a temperature range of –35 to 0°C showed the model capable of predicting the ΔT of tank tracks with an accuracy of ±1°C (Jordan et al. 1989). SNTHERM.89 marks a major extension to the model, incorporating the mass balance features described in the preceding paragraphs and addressing metamorphism of the snow pack. Water flow is limited to snow, for which an appropriate gravity flow algorithm is used. An expanded model, SNTHERM2, which is currently in production, includes capillary flow in soil, redistribution of water towards a freezing front, ponding, saturated flow and a two-stream radiative transfer algorithm for computing albedo and solar absorption. The present version, SNTHERM.89, which has been released as an interim model, contains material still under development, as noted in the subsequent discussion. The purpose of this report is to provide technical documentation in support of the limited distribution of the SNTHERM.89 code. An expanded and more in-depth publication (Jordan, in prep.) will accompany the release of SNTHERM2.

Early development of the CRREL model drew extensively from the thorough and definitive study of Anderson (1976). Later versions have employed the mixture theory approach espoused by Morris and Godfrey (1979) and Morris (1987), which has recently been given a rigorous theoretical framework by Morland et al. (1990). The treatment of water flow within the snow pack is taken from Colbeck (1971, 1972, 1976, 1979).

Outline of the report

The outline of this report is as follows. The next section provides a general description of porous media and sets forth the basic mixture theory and terminology that are used in the model. The following section is devoted to aspects of mass balance, first establishing the basic numerical approach and then developing the continuity and fluid flow equations. Also included in this section are discussions of snowfall accumulation, snow cover compaction and grain growth. The energy-balance equation and phase-change algorithm are then presented, along with the related issues of solar extinction in snow, turbulent exchange across the air interface, and estimation of radiation fluxes. The last major section is devoted to the numerical implementation of the conservation equations and to a description of the overall structure of the model. The remaining shorter sections present examples of model verification and the concluding remarks.

BASIC DEFINITIONS

Snow and soil are examples of porous media, which are characterized by a solid, immobile matrix and an interstitial system of more or less evenly distributed voids. They are mathematically described here by mixture theory, which takes into account the constituent mix of the material and the interfacial relationships among the phases. In the case of snow the matrix is composed of ice, and in soil, of the dry solids. In contrast to snow the ice component of frozen soil is considered to be mobile and detached from the supporting matrix. The void space in snow or soil is completely occupied by an immiscible mixture of fluids, composed of air, liquid water and mobile ice. Air is further subdivided into miscible dry and moist components. Whereas dry air is relatively inactive in the thermal process, water vapor consumes an appreciable amount of heat upon sublimation and is considered as a separate component. Dry air, the dry soil solids and the three phases of water will therefore constitute the mixture under study. At this stage of development, contaminants are not taken into account. Within the snow or soil medium, all five constituents are assumed to be in local thermal equilibrium, and in the limit of a one-dimensional study the medium is considered to be horizontally homogeneous.

With the objective of a unified approach adaptable to either medium, the simplified mixture theory presented here can be applied to soil or snow. On a spatial scale of centimeters, the media approach a continuum and can be described by bulk properties. Using the terminology of mixture theory (Morris 1987, Morland et al. 1990), the partial or bulk density γ_k is introduced to denote the mass of constituent k per unit volume of medium, where the subscript k becomes v, ℓ, i, a or d for water vapor, liquid water, ice, air or the dry soil solids, respectively. Intrinsic density ρ_k is defined as the mass of constituent k per unit volume of constituent k and is related to bulk density as

$$\gamma_k = \theta_k \rho_k \tag{1}$$

where θ_k is the volume fraction or partial volume (m^3/m^3) of constituent k, and γ_k and ρ_k are in kg/m^3. Taken over the five possible constituents in the medium, the sum of the volume fractions is unity, or

$$\sum_k \theta_k = 1 \, . \tag{2}$$

The sum of the constituent bulk densities is the density ρ_t of the total medium, written as

$$\rho_t = \sum_k \theta_k \rho_k = \sum_k \gamma_k \, . \tag{3}$$

Since the mass of air is less than 1% of the snow mixture, the density of snow ρ_s and the bulk density of the combined liquid water and ice constituents ($\gamma_w = \gamma_\ell + \gamma_i$) are nearly equal in magnitude and will often be referred to interchangeably. Because mixture theory is consistently applied in the development of the model, the mathematical structure is very flexible. By changing the specified volume fractions or volumetric mix, it is possible to simulate a variety of terrain features, such as ice fields, lakes and pavements, as well as snow and soil, with the same basic set of equations.

Porosity ϕ is a measure of the space within a medium available to fluids and is defined as the ratio of the pore volume to the total volume (m^3/m^3). Since the supporting matrices of snow and soil are made up of ice and dry solids, the porosities of these two materials are defined as

$$\phi = 1 - \theta_i = 1 - \frac{\gamma_i}{\rho_i} \tag{4a}$$

for snow and

$$\phi = 1 - \theta_d = 1 - \frac{\gamma_d}{\rho_d} \tag{4b}$$

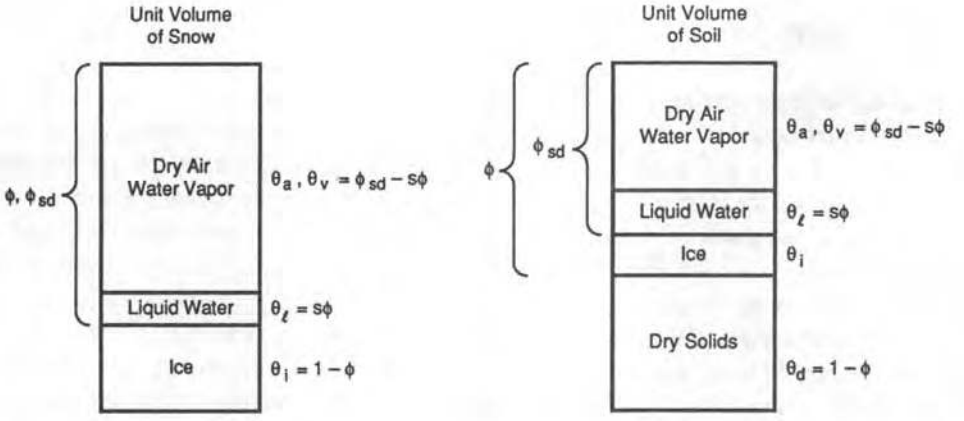

Figure 1. Fractional volume relationships in snow and soil. The air portion includes dry and wet (water vapor) components.

for soil. An alternative quantity, termed the "solid" porosity ϕ_{sd} (where the subscript *sd* refers to solid), will be used to refer to voids between the solids (ice plus dry solids) and is written as

$$\phi_{sd} = 1 - \frac{\gamma_i}{\rho_i} - \frac{\gamma_d}{\rho_d} . \tag{5}$$

In practice, only the interconnected pore space is available to fluid flow, which is not accounted for in the preceding definitions.

Volume fractions θ_k can be expressed in terms of the porosity and the liquid saturation s, where the latter is defined as the volume of liquid water per unit volume of voids (m^3/m^3). The following frequently used relationships, noted here for reference, are illustrated in Figure 1:

$$\begin{aligned} \theta_i &= 1 - \phi \quad \text{(for snow)} \\ \theta_\ell &= s\,\phi \\ \theta_a &= \phi_{sd} - s\phi \\ \theta_v &= \phi_{sd} - s\phi . \end{aligned} \tag{6}$$

MASS AND MOMENTUM BALANCE

General theory and numerical method

Heat and fluid flow within porous media are governed by conservation equations for mass, momentum and energy. Within a finite control volume ΔV, the time rate of change in these quantities must equal their net flow across the bounding surface dS, plus their rate of internal production. Using the control-volume method espoused by Patankar (1980, p. 30–31), the equations are formulated here in integral form, subject to assumed profiles for the physical quantities within ΔV. This method lends itself to direct physical interpretation, in that quantities are in theory conserved over ΔV rather than at an infinitesimal point as with a finite-difference scheme.

The numerical solution is obtained by subdividing the snow and underlying soil into n horizontally infinite plane-parallel control volumes of area A and variable thickness Δz, as shown in Figure 2. Contrary to usual practice, these are indexed in ascending order from the bottom up, which permits

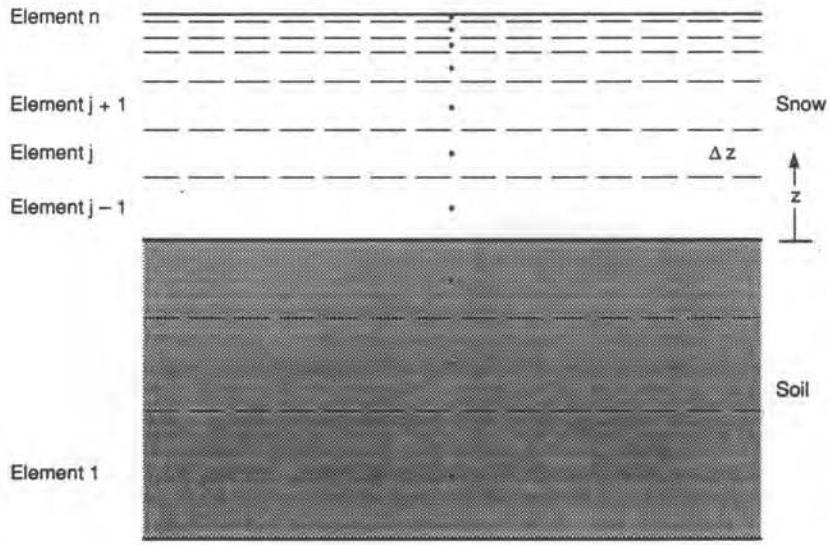

Figure 2. Finite-difference grid.

the accumulation or ablation of snow at the top of the snow cover without renumbering the elements. Generally speaking, the grid is constructed so that volume boundaries correspond to the natural layering of the snow cover, which assures that assumptions of nodal homogeneity are realistically met. As snow compacts over time, the grid is allowed to compress, so that the volume elements continue to correspond with the original sample of snow. Thus the parameter z is not strictly a spatial coordinate but rather specifies the nodal position relative to the snow/soil interface. The velocity of the fluxes is taken with respect to the deforming grid and is positive in the upward direction.

In accordance with the control volume approach, conservation equations are expressed in integral form as

$$\frac{\partial}{\partial t}\int_V \gamma_k \Omega \, dV = -\overline{\sum_k \int_S \mathbf{J} \cdot d\mathbf{S}} + \int_V \overline{S \, dV} \qquad (7)$$

time rate of change — fluxes — source term

where k = i, ℓ, v and a
Ω = quantity being conserved
$\mathbf{J}$ = flux
S = source density.

The overbars indicate a temporal average over the time step (Δt). Based on assumed profiles for the various physical quantities, the integrals are then evaluated over the control volume ($\Delta V = A\Delta z$). If physical quantities are taken as stepwise-homogeneous, the mean and nodal values of Ω are the same and the control volume formulation reduces to the more commonly used finite-difference method (Smith 1978, Albert 1983). The terms "element," "node" and "control volume" will henceforth be used interchangeably but in a strictest sense refer to the control volume. As in any finite description, the approximate solution must converge to the actual solution as the grid spacing becomes sufficiently small.

If Ω, γ_k and S are homogeneous over ΔV, eq 7 integrates to

$$\frac{\partial}{\partial t}\gamma_k \Omega \Delta z = -\sum_k \overline{\left[J^{*j+\frac{1}{2}} - J^{*j-\frac{1}{2}}\right]} + \overline{S\Delta z} \qquad (8)$$

time rate of change | fluxes | source term

where j = nodal index

k = i, ℓ, v and a

$j^{+\frac{1}{2}}$ = index referring to the upper bounding surface of the control volume.

$j^{-\frac{1}{2}}$ = index referring to the lower bounding surface of the control volume.

Note that the elemental thickness Δz is left within the derivative. The quantity $\gamma_k \Delta z$ (kg/m^2) will henceforth be referred to as a mass, although it is actually normalized per unit area. The asterisk on the flux term J^* indicates that it may be either convective or diffusive or a combination of both processes. Within the temporal domain a Crank–Nicolson weighting scheme is used, which implies that quantities vary linearly with time over Δt. The temporal average for any quantity χ is therefore expressed as

$$\overline{\chi} = 0.5\left[\chi^{t-\Delta t} + \chi^t\right] \qquad (9)$$

where $\chi^{t-\Delta t}$ and χ^t are the past and current values. Henceforth, an overbar indicates an average as stated in eq 9. The iterative time step ranges between user-specified maximum and minimum values (usually 900 and 5 s) and is adjusted automatically by the program so that the desired solution accuracy is met, as discussed later. If we assume that liquid water is dragged along by the compacting ice matrix, the partial masses of the ice and liquid water constituents are conserved during compression, so that for an incremental change in time, $(\gamma_k \Delta z)^t = (\gamma_k \Delta z)^{t-\Delta t}$. The densities of water vapor and dry air, however, remain invariant during matrix deformation. A portion of gas is expelled from the contracting volume, which must be taken into account when defining the fluxes for these constituents.

In evaluating the surface integral for the fluxes, it is assumed that the profile of Ω is piecewise-linear for a diffusive–conductive process and stepwise for a convective process. The former leads to a central difference scheme of the form (Smith 1978, Albert 1983)

$$\text{net conductive–diffusive flux} = \overline{\left[J^{j+\frac{1}{2}} - J^{j-\frac{1}{2}}\right]} = -\overline{\left[\left(D\frac{\partial \Omega}{\partial z}\right)^{j+\frac{1}{2}} - \left(D\frac{\partial \Omega}{\partial z}\right)^{j-\frac{1}{2}}\right]} \qquad (10)$$

where D is a diffusion coefficient. The latter leads to an upwind scheme (Patankar 1980), written as

$$\text{net convective flux} = \overline{\left[J^{j+1} - J^j\right]} = \overline{\left[(U\Omega)^{j+1} - (U\Omega)^j\right]} \qquad (11)$$

in which U is a mass flux. Conductive–diffusive fluxes at the control volume boundaries are denoted by $J^{j+\frac{1}{2}}$ and $J^{j-\frac{1}{2}}$ (with the asterisk omitted), and convective fluxes by J^{j+1} and J^j. In the latter scheme the flux has the value of the upwind element, which makes it an appropriate method when gravitational flow dominates, as is generally the case with water flow through snow.

Equations for mass balance

For a given time step, solutions to the mass and energy balance equations are obtained sequentially, with the fluid flows being determined first and subsequently coupled to the energy equation. The mass balance equations apply simultaneously to the total medium and the individual constituents. In integral form the mass conservation equation for the medium is expressed as

$$\frac{\partial}{\partial t}\int_V \rho_t \, dV = -\overline{\sum_k \int_S \mathbf{U}_k^* \cdot d\mathbf{S}} \tag{12}$$

where k = i, ℓ, v and a and $\mathbf{U}_k^*$ represents mass fluxes corresponding to flows of falling snow or ice, liquid water, water vapor and air, defined as

$$\mathbf{U}_k^* = \rho_k \theta_k \mathbf{v}_k = \gamma_k \mathbf{v}_k \tag{13}$$

where $\mathbf{v}_k$ is the seepage velocity vector (m/s) and the asterisk indicates that the flux may be either diffusive or convective. All quantities, including the total density ρ_t and the control volume ΔV, are assumed to vary with time. Similarly, conservation equations can be written for each of the water phases as

$$\frac{\partial}{\partial t}\int_V \gamma_k \, dV = -\overline{\int_S \mathbf{U}_k^* \cdot d\mathbf{S}} + \sum_{k'} \int_V \overline{M_{k'k} \, dV \left(1 - \delta_{k'k}\right)} \tag{14a}$$

where k, k′ = i, ℓ and v and for dry air as

$$\frac{\partial}{\partial t}\int_V \gamma_a \, dV = -\overline{\int_S \mathbf{U}_a^* \cdot d\mathbf{S}} \cdot \tag{14b}$$

The variable $\delta_{k'k}$ is the Kronecker delta, the source terms $M_{\ell i}$, M_{vi} and $M_{v\ell}$ denote the mass rates of melt, sublimation and evaporation (kg/m^3·s), and

$$M_{k\,k'} = -M_{k'k} \cdot \tag{15}$$

At this stage in model development, the soil matrix is taken as immobile and incompressible and therefore does not require a constituent equation. Air is assumed to be incompressible, stagnant and at atmospheric pressure throughout the pore space. For this version of the model, its effect on water flow is not considered. Furthermore, since only latent heat changes are retained for the gaseous constituents, mass changes in dry air are henceforth neglected. If flows are constrained to the vertical direction and the bulk densities and source terms are assumed to be constant over ΔV, eq 12 and 14 become

$$\frac{\partial}{\partial t}\gamma_t \, \Delta z = -\sum_k \overline{\left(U_k^{*\,j+\frac{1}{2}} - U_k^{*\,j-\frac{1}{2}}\right)}$$

where k = i, ℓ and v, and

$$\frac{\partial}{\partial t}\gamma_k \Delta z = -\overline{\left(U_k^{*\,j+\frac{1}{2}} - U_k^{*\,j-\frac{1}{2}}\right)} + \sum_{k'} \overline{M_{k'k} \, \Delta z \left(1 - \delta_{k'k}\right)} \tag{16}$$

where k, k′ = i, ℓ and v. Although the assumption of negligible free convection of air seems reasonable for a seasonal snow cover, there are indications of enhanced thermal conductivity at the top of the snowpack during moderate to high winds. The effects of forced convection due to windpumping on heat transfer within snow warrants further investigation (Colbeck 1989).

Ignoring the convective flux for water vapor and taking into account vapor expelled from the contracting control volume, we can write the continuity equation for water vapor as*

$$\underbrace{\frac{\partial \gamma_v \Delta z}{\partial t}}_{\text{expulsion vapor flux}} - \underbrace{\overline{\rho}_v \frac{\partial \theta_v \Delta z}{\partial t}}_{\text{diffusive vapor flux}} = \underbrace{\overline{\left(D_e \frac{\partial \rho_v}{\partial z}\right)^{j+\frac{1}{2}} - \left(D_e \frac{\partial \rho_v}{\partial z}\right)^{j-\frac{1}{2}}}}_{\text{sources and sinks}} + \overline{M_{vi} \Delta z} + \overline{M_{v\ell} \Delta z} \qquad (17)$$

where D_e is an effective diffusion coefficient (m^2/s). Water vapor within the pores is assumed to be at equilibrium with respect to water if the liquid water content exceeds the arbitrary level of 0.02, and otherwise to be at equilibrium with respect to ice, giving

$$\gamma_v = \theta_v \rho_v = \theta_v f_{rh} \rho_{vk,\,sat} \qquad (18)$$

where k = i if $\theta_\ell \le 0.02$ and k = ℓ if $\theta_\ell > 0.02$, and the subscript vk,sat refers to vapor saturation with respect to water or ice. The fractional humidity f_{rh} is assumed constant over the simulation and is taken as 1.0 for snow and as ≤ 1.0 for soil. In order that equilibrium levels be maintained, continuity requires that vapor flows across the control volume boundaries be compensated by phase gains and losses within the medium. Applying the chain rule, we can rewrite the time and spatial partial derivatives of the vapor density as

$$\frac{\partial \rho_{vk,\,sat}}{\partial t} = C_{kT} \frac{\partial T}{\partial t} \quad \text{and} \quad \frac{\partial \rho_{vk,\,sat}}{\partial z} = C_{kT} \frac{\partial T}{\partial z} \qquad (19)$$

where k = i if $\theta_\ell \le 0.02$ and k = ℓ if $\theta_\ell > 0.02$. The variation of equilibrium vapor density with temperature C_{kT} is expressed as

$$C_{kT} = \frac{\partial \rho_{vk,\,sat}}{\partial T} = \frac{c1_k}{T^2}\left[\frac{L_{vk}}{R_w T} - 1\right] e^{-\left(\frac{L_{vk}}{R_w T}\right)} \qquad (20)$$

where k = i if $\theta_\ell \le 0.02$
k = ℓ if $\theta_\ell > 0.02$
$L_{v\ell}$ = latent heat of evaporation for water (2.505×10^6 J/kg)
L_{vi} = latent heat of sublimation for ice (2.838×10^6 J/kg)
R_w = gas constant for water vapor (461.296 J/kg·K)

$$c1_\ell = \frac{100 P_{v0,\,sat}\, e^{\left(\frac{L_{v\ell}}{R_w T_0}\right)}}{R_w} = 5.726 \times 10^8 \text{ kg/m}^3\text{·K}$$

$$c1_i = \frac{100 P_{v0,\,sat}\, e^{\left(\frac{L_{vi}}{R_w T_0}\right)}}{R_w} = 8.047 \times 10^9 \text{ kg/m}^3\text{·K}$$

$P_{v0,sat}$ = saturation vapor pressure at T_0 = 273.15 K (6.1360 mb).

Now, if the mass vapor flux U_v (kg/m^{-2}·s) is defined as (Anderson 1976,† Farouki 1981)

---

*The diffusive vapor flux in snow is customarily taken as independent of porosity, which is generally a consequence of the "hand-to-hand" process of vapor diffusion.

†The exponential power on temperature in eq 21 was determined through a curve fit to the data of Yen (1963) and Yoshida (1950), where the mean values were $D_e = 0.65 \times 10^{-4}$ m^2/s and $T = -15.4$°C, and $D_e = 0.8 \times 10^{-4}$ m^2/s and $T = -4$°C, respectively. Further investigation of this temperature relationship is needed.

$$U_v = -D_{es} C_{kT} \frac{\partial T}{\partial z} = -D_{eos} \left(\frac{1000}{P_a}\right)\left(\frac{T}{273.15}\right)^6 C_{kT} \frac{\partial T}{\partial z} \tag{21}$$

for snow and

$$U_v = -D_{eg} f_{rh} C_{kT} \frac{\partial T}{\partial z} = -D_{eog} \left(\frac{1000}{P_a}\right)\left(\frac{T}{273.15}\right)^{2.3} f_{rh} C_{kT} \frac{\partial T}{\partial z}$$

for soil

where P_a = atmospheric pressure (mb)
D_{es} and D_{eg} = effective diffusion coefficients for snow and soil
D_{e0s} and D_{e0g} = effective diffusion coefficients at 1000 mb and 0°C

then the media and constituent continuity equations for the interior elements are written as*

$$\frac{\partial}{\partial t}(\rho_t \Delta z) - \overline{\rho_{vk,sat} f_{rh}} \frac{\partial(\theta_v \Delta z)}{\partial t} = -\overline{\left(U_\ell^{j+1} - U_\ell^j\right)} - \overline{\left(U_v^{j+\frac{1}{2}} - U_v^{j-\frac{1}{2}}\right)} \tag{22}$$

for the total media,

$$\frac{\partial}{\partial t}(\gamma_i \Delta z) = -\overline{M_{\ell i} \Delta z} - \overline{M_{vi} \Delta z} \tag{23}$$

for ice,

$$\frac{\partial}{\partial t}(\gamma_\ell \Delta z) = -\left(\overline{U_\ell^{j+1} - U_\ell^j}\right) + \overline{M_{\ell i} \Delta z} - \overline{M_{v\ell} \Delta z} \tag{24}$$

for liquid water and

$$\overline{(\Phi_{sd} - s\Phi)\Delta z}\ \overline{f_{rh} C_{kT}} \frac{\partial T}{\partial t} = -\left(\overline{U_v^{j+\frac{1}{2}} - U_v^{j-\frac{1}{2}}}\right) + \overline{M_{vi} \Delta z} + \overline{M_{v\ell} \Delta z} \tag{25}$$

for water vapor, where $M_{v\ell} = 0$ if $\theta_\ell \leq 0.02$ and $M_{vi} = 0$ if $\theta_\ell > 0.02$, and U, without the asterisk, refers to diffusive–conductive or convective mass fluxes as noted earlier for the generalized fluxes J (eq 10 and 11). As discussed later, gravitational flow is assumed in describing the movement of water through snow, and an upwind scheme is used for U_ℓ. Snowfall has been omitted from eq 23, since it is constrained to the top node, as discussed in the section on boundary conditions for mass and momentum flow.

Snow compaction and granular growth rate

Immediately upon reaching the ground, snow begins a process of rapid change in which individual snowflakes quickly lose their original shape and metamorphose into more rounded forms. Branched crystals break down, either through the mechanical forces of wind or through thermodynamic stress, so that settling or grain packing of the snow pack occurs. As snow accumulates, the weight of overlying snow results in a further, more sustained, compaction of the snow cover. Stress from the overburden

* In the SNTHERM.89 version, mass changes due to vapor diffusion in soil have been temporarily disallowed except for the top element. Evaporation from the top node is not permitted when the water content reaches the irreducible saturation limit for that soil type.

leads to an increased rate of bond growth, which in turn results in grain shapes that pack more efficiently (Colbeck 1973). The greatest changes occur immediately after snow has fallen, when, on average, density increases at 1% per hour (Gunn 1965, as reported in Anderson 1976). This rate increases by at least an order of magnitude for intense snowfalls of soft snow (Mellor 1977) or when there are strong winds. Under blizzard conditions with winds over 17 m/s, the density of new snow has been found to increase from 45 to 230 kg/m^3 within a 24-hour period (Gray 1979).

Following the approach of Anderson (1976, p. 36–39, 82–83), the snow compaction process will be considered in two stages. For newer snow with densities of less than 150 kg/m^3, settling due to destructive metamorphism is important. New snow has a certain structural strength due to "cogging" between the crystal branches, which gives way as metamorphism proceeds (deQuervain 1963). Anderson proposed the following empirical function for compaction at this stage:

$$\left[\frac{1}{\Delta z}\frac{\partial \Delta z}{\partial t}\right]_{\text{metamorphism}} = -2.778 \times 10^{-6} \times c3 \times c4 \times e^{-0.04\,(273.15 - T)} \tag{26}$$

where $c3 = c4 = 1$ if $\gamma_\ell = 0$ and $\gamma_i \leq 150$ kg/m^3
$c3 = \exp^{[-0.046\,(\gamma_i - 150)]}$ if $\gamma_i > 150$ kg/m^3
$c4 = 2$ if $\gamma_\ell > 0$.

Note that eq 26 predicts a deformation rate of 1% per hour for snow densities less than 150 kg/m^3 and has an enhancement factor of two for wet snow.

After snow has undergone its initial settling stage, densification proceeds at a slower rate, which is largely determined by the snow load or overburden. In the low stress range associated with seasonal snow covers, the deformation rate is a linear function of the snow load pressure P_s such that

$$\left[\frac{1}{\Delta z}\frac{\partial \Delta z}{\partial t}\right]_{\text{overburden}} = -\frac{P_s}{\eta} \tag{27}$$

where P_s is in N/m^2 and η is a viscosity coefficient (N· s/m^2) that varies with density, temperature and grain type. The viscosity coefficient, which increases exponentially as the load pressure and snow density come into hydrostatic equilibrium, has been found by observation to take the form (Mellor 1964, Kojima 1967, as reported by Anderson)

$$\eta = \eta_0\, e^{c5(273.15 - T)}\, e^{c6\rho_s} \tag{28}$$

where η_0 is the viscosity coefficient at $T = 273.15$ K and $\rho_s = 0$. By substituting into eq 27, we can express the compaction rate for snow of density ρ_s subject to a load pressure P_s as

$$\left[\frac{1}{\Delta z}\frac{\partial (\Delta z)}{\partial t}\right]_{\text{overburden}} = \frac{-P_s}{\eta_0}\, e^{-c5\,(273.15 - T)}\, e^{-c6\rho_s}. \tag{29}$$

Based on reported measurements by Mellor and Kojima, Anderson suggested values for the parameters of $\eta_0 = 3.6 \times 10^6$ N· s/m^2, $c5 = 0.08$ K^{-1} and $c6 = 0.021$ m^3/kg. Equations 26 and 29 are combined to obtain a total fractional compaction rate CR of

$$CR \equiv -\frac{1}{\Delta z}\frac{\partial \Delta z}{\partial t} = -\left[\frac{1}{\Delta z}\frac{\partial \Delta z}{\partial t}\right]_{\text{metamorphism}} - \left[\frac{1}{\Delta z}\frac{\partial \Delta z}{\partial t}\right]_{\text{overburden}} \tag{30}$$

Substitution of this function into the continuity equation (eq 22) provides an expression for the overall densification of the snow cover:

$$\frac{\partial \rho_s}{\partial t} = \frac{\left[\overline{\rho_{vk,\,sat} f_{rh}} \frac{\partial (\theta_v \Delta z)}{\partial t} - \overline{\left(U_\ell^{j+1} - U_\ell^{j}\right)} - \overline{\left(U_v^{j+\frac{1}{2}} - U_v^{j-\frac{1}{2}}\right)} + \overline{CR}\ \overline{\rho_s}\ \overline{\Delta z}\right]}{\overline{\Delta z}} . \quad (31)$$

In addition to the effects of compaction, eq 31 takes into account grain growth due to vapor movement (constructive metamorphism) and densification from water flow. Anderson has verified his densification algorithm with snow observations from five winter seasons, and it shows excellent agreement between theory and measurements (Anderson 1976, p. 88–93). His settling function does not take into account the effects of wind, which would be a beneficial refinement for the future.

Grain size is a critical variable in both the mass and energy balance equations, in that it affects (among other things) the permeability of snow to fluid flow and the extinction coefficient for solar radiation. Stephenson (1967, reported in Wiscombe and Warren 1980) proposed grain diameters in the range of 0.04–0.2 mm for new snow, 0.2–0.6 mm for fine-grained older snow and 2.0–3.0 mm for older snow near 0°C. The processes of crystal growth within a snow cover are complex and subject to debate, although work by Colbeck (1982, 1983a, 1983b and 1987) and Gubler (1985) have advanced understanding in the area.

Within dry snow, grain growth is generally a result of the upward moving "hand-to-hand" vapor flux, in which vapor condenses on the bottom and evaporates from the top of snow grains (Yoshida 1963). Since the vapor pressure is higher for smaller particles, they tend to be consumed or cannibalized by larger particles (Colbeck 1973), leading to an overall upward shift in the particle size distribution with time. A theoretically based thermodynamic growth function is beyond the current scope of this study but will be addressed in a subsequent version of the model. Based on observations of grain growth metamorphism in Antarctica, Stephenson (1967) and Gow (1969) (as reported in Wiscombe and Warren 1981) have had success with a function that is used to predict growth by sintering in metals and ceramics:

$$d\frac{\partial d}{\partial t} = a\, e^{-(b/T)} \quad (32)$$

where d = mean grain diameter (m)
T = temperature (K)
a, b = adjustable variables.

I propose for use here, as an interim formulation, a simple function of the form

$$\frac{\partial d}{\partial t} = \frac{g1\,|U_v|}{d} = \frac{g1}{d} D_{eos} \left(\frac{1000}{P_a}\right)\left(\frac{T}{273.15}\right)^6 C_{kT} \left|\frac{\partial T}{\partial z}\right| \quad (33)$$

where the mass vapor flux U_v (kg/m^2 · s) provides the necessary vapor source for growth and the inverse relation $1.0/d$ is in agreement with the observed slowing of the growth rate with increased particle size. Further refinement of the relationship is needed, but preliminary comparison with data suggests a value on the order of 5.0×10^{-7} m^4/kg for the adjustable variable $g1$. Because of the inherent temperature relationships in the diffusion function, eq 33 predicts an increased growth rate at higher temperatures and higher thermal gradients. For a snow temperature of –2°C and a thermal gradient of 10°C/m, the predicted size of a 0.5-mm particle after 30 days is approximately 1 mm. Note that the vapor flux as it is used here assumes a purely diffusive process, as defined in eq 21, and that eq 33 is not appropriate when a convective component is present.

Within wet snow, there is a marked increase in grain growth for "even small quantities of water" (Colbeck 1982), which increases even further for water saturations in the funicular regime. The

equilibrium fusion temperature is higher for larger particles than for smaller particles, so that growth of larger grains in the distribution is fed by meltwater from the disappearing smaller grains. A similar growth function is proposed to that for dry snow:

$$\frac{\partial d}{\partial t} = \frac{g2}{d}\left(\theta_\ell + 0.05\right) \tag{34a}$$

when $0.00 < \theta_\ell < 0.09$ and

$$\frac{\partial d}{\partial t} = \frac{g2}{d}\,(0.14) \tag{34b}$$

when $\theta_\ell \geq 0.09$, where $g2$ is an adjustable variable and the growth rate increases with the liquid water fraction up to the start of the funicular regime at $s \approx 0.14$. Observations of the particle size distributions in liquid-saturated snow have been made by Wakahama (1965, reported in Colbeck 1982 and Colbeck 1986), who reported increases in mean grain size from about 0.3 to 0.8 mm in six days, and from 0.21 to 1.78 mm in 1028 hours, respectively. For a liquid volume fraction of 0.09, an approximate fit to these data provides a value of 4.0×10^{-12} m^2/s for $g2$.*

Momentum balance and fluid flow

The movement of fluids through a porous medium results from the combined action of gravitational, viscous and surface stress or pressure forces. In accordance with Newton's second law for continuous media, the rate of change in momentum within the control volume equals the net flux across its bounding surface plus the resultant force on the fluid plus the momentum generated through phase change. Within snow or soil media, flow of both the water and air phases is present, although only the water phase will be considered here. The integral momentum equation for an isotropic medium and a Newtonian fluid undergoing negligible divergence can be written as†

$$\underbrace{\frac{\partial}{\partial t}\int_V \gamma_\ell\, \mathbf{v}_\ell \, dV}_{\text{inertial term}} + \underbrace{\int_S \overline{\mathbf{U}_\ell^*\, \mathbf{v}_\ell \cdot d\mathbf{S}}}_{\text{convection}} = \underbrace{-\,\theta_\ell \int_S \overline{P_\ell\, \mathbf{i} \cdot d\mathbf{S}}}_{\text{pressure}}$$

$$\underbrace{-\int_V \overline{\left(-\gamma_\ell \mathbf{g} + \frac{\theta_\ell^2\, \mu_\ell\, \mathbf{v}_\ell}{K_\ell}\right) dV}}_{\text{gravity}\quad\text{viscous stress}} + \underbrace{\int_V \overline{\left(M_{\ell \mathrm{i}} \frac{\mathbf{v}_\ell + \mathbf{v}_\mathrm{i}}{2} - M_{\mathrm{v}\ell} \frac{\mathbf{v}_\mathrm{v} + \mathbf{v}_\ell}{2}\right)} dV}_{\text{phase change}} \tag{35}$$

where $\mathbf{g}$ = gravitational vector, positive downwards (m/s^2)
P_ℓ = intrinsic pressure (N/m^2)
μ_ℓ = dynamic viscosity (N·s/m^2)
K_ℓ = hydraulic permeability (m^2)
$\mathbf{i}$ = unit vector (m).

---

* Values for $g1$ and $g2$ are preliminary and need to be evaluated with further field data.

† The presentation here of the momentum equation is simplified and does not contain a complete description of the interactive forces between the constituents. For a more thorough treatment, see the papers of Morris (1987) and Morland et al. (1990).

The seepage velocity vector $\mathbf{v}_\ell$ is in effect an average over the point velocities of the fluid particles within the medium. Again the problem is reduced to that of one-dimensional vertical flow, and γ_k, M_{jk}, θ_k, K_ℓ and $\mathbf{v}_\ell$ are taken as constant over Δz. Integrating over the control volume $A\Delta z$ and employing the divergence theorem to convert the surface integral in the pressure term to a volume integral, we can write eq 35 as

$$\rho_\ell \left[\frac{\partial v_\ell}{\partial t} + \overline{v}_\ell \frac{\overline{\left(v_\ell^{\,j+\frac{1}{2}} - v_\ell^{\,j-\frac{1}{2}}\right)}}{\Delta z} \right] = - \frac{\overline{\left(P_\ell^{\,j+\frac{1}{2}} - P_\ell^{\,j-\frac{1}{2}}\right)}}{\Delta z} - \rho_\ell g - \frac{\overline{\theta_\ell \mu_\ell v_\ell}}{K_\ell}$$

$$- \frac{1}{2} \frac{\overline{\left[M_{\ell i}(\mathbf{v}_\ell - \mathbf{v}_i) + M_{v\ell}(\mathbf{v}_v - \mathbf{v}_\ell)\right]}}{\theta_\ell} . \tag{36}$$

The left-hand terms have been simplified by applying the product rule:

$$\frac{\partial}{\partial t}(\gamma_\ell v_\ell \Delta z) + \overline{\left(v_\ell U_\ell^*\right)^{j+\frac{1}{2}} - \left(v_\ell U_\ell^*\right)^{j-\frac{1}{2}}} =$$

$$\overline{v}_\ell \left[\frac{\partial}{\partial t}(\gamma_\ell \Delta z) + \overline{U_\ell^{*\,j+\frac{1}{2}} - U_\ell^{*\,j-\frac{1}{2}}} \right] + \overline{\gamma}_\ell \left[\overline{\Delta z} \frac{\partial v_\ell}{\partial t} + \overline{v}_\ell \overline{\left(v_\ell^{\,j+\frac{1}{2}} - v_\ell^{\,j-\frac{1}{2}}\right)} \right] \tag{37}$$

where by using the continuity equation for liquid water (eq 24), the first term of the right in eq 37 equals $\overline{v_\ell}\left(\overline{M_{\ell i}\Delta z} - \overline{M_{v\ell}\Delta z}\right)$. If we assume that the inertial, convective and phase change terms are small (Corey 1977, p. 76, Morris 1987, p. 191–192) and that the air is at atmospheric pressure, eq 36 for the water phase simplifies to

$$\theta_\ell v_\ell = - \frac{K_\ell}{\mu_\ell} \left[\rho_\ell g - \frac{\left(p_{a\ell}^{\,j+\frac{1}{2}} - p_{a\ell}^{\,j-\frac{1}{2}}\right)}{\Delta z} \right] \tag{38}$$

which is in the form of the empirically derived Darcy equation, in which water pressure is expressed in terms of the capillary pressure, $p_{a\ell} = P_a - P_\ell$. Furthermore, since capillary forces within snow are usually two to three orders of magnitude less than those of gravity (Colbeck 1971, p. 3), the equation for the mass water flux in snow reduces to the gravitational form*

$$U_\ell = \rho_\ell \theta_\ell v_\ell = - \frac{K_\ell}{\mu_\ell} \rho_\ell^2 g \tag{39}$$

which is discretized by the upwind scheme as presented in eq 11.

Hydraulic permeability is a measure of the ease and rate at which water is transmitted by a medium and is generally expressed in terms of the effective liquid saturation s_e, which is defined as

$$s_e = \frac{s - s_r}{1 - s_r} \tag{40}$$

where s_r is the irreducible water saturation, or the minimum liquid level to which a snow cover can be

---

* As Colbeck points out (1971, p. 3 and 13), the assumption that $\partial P_\ell / \partial z$ is small is not valid at a shock front. Subsequent versions of the model will retain the capillary term.

drained regardless of the imposed suction (Colbeck 1972). For estimating K_ℓ the formula of Brooks and Corey (1964) is used:

$$K_\ell = K_{\max}\, s_e^{\varepsilon} \tag{41}$$

where the exponent ε depends on the pore size distribution, and $K_{\max}$ (m^2) is the saturation permeability, approximated from the relationship of Shimizu (1970), as

$$K_{\max} = 0.077\ d^2 e^{(-0.0078\,\gamma_i)}. \tag{42}$$

Based on field data of water flow through a ripe snowpack, Colbeck and Anderson (1982) suggested a value of 3 for ε. Expressing the saturation s in terms of s_e

$$s = s_e(1 - s_r) + s_r \tag{43}$$

and noting that $\gamma_\ell = \rho_\ell s\phi$, we can express the change in liquid water mass $\partial\gamma_\ell\Delta z/\partial t$ as

$$\frac{\partial(\gamma_\ell \Delta z)}{\partial t} = \rho_\ell \frac{\partial(s\phi\Delta z)}{\partial t} = \rho_\ell (1 - s_r)\,\overline{\phi\Delta z}\,\frac{\partial s_e}{\partial t} + \rho_\ell\,\bar{s}\,\frac{\partial\phi\Delta z}{\partial t}\,. \tag{44}$$

Discounting sublimation changes, the continuity equation for ice (eq 23) gives the following relationship for the change in porosity of snow:

$$\frac{\partial(\phi\Delta z)}{\partial t} = \frac{\overline{M_{\ell i}\Delta z}}{\rho_i} + \frac{\partial\Delta z}{\partial t}\,. \tag{45}$$

Now substituting into the continuity equation for water (eq 24) and employing the upwind scheme for U_ℓ, we can write the final form of the fluid flow equation as*

$$\rho_\ell(1-s_r)\,\overline{\phi\Delta z}\,\frac{\partial s_e}{\partial t} = \frac{\rho_\ell^2\, g}{\mu_\ell}\left[\overline{(K_{\max} s_e^3)}^{j+1} - \overline{(K_{\max} s_e^3)}^{j}\right] + \overline{M_{\ell i}\Delta z}\left(1 - \frac{\rho_\ell \bar{s}}{\rho_i}\right) - \rho_\ell\,\bar{s}\,\frac{\partial\Delta z}{\partial t} \tag{46}$$

Since the residual saturation deficit must be satisfied prior to the advancement of the water front, the parameter s_r is critical in determining the infiltration rate and the equilibrium liquid water content. Based on a drainage curve of kerosene and snow, Colbeck (1974b) suggested a value of $s_r = 0.07$. A compendium of data from different researchers using various procedures (Kattelmann 1986) shows a broad range from 0.0 to 0.4 for the irreducible water content $\theta_r = s_r\phi$, with most values lying between 0.01 and 0.05. For a snow of density 250 kg/m^3 the porosity is 72%, and s_r correspondingly lies between 0.014 and 0.069. Although higher values of θ_r are generally associated with newer snow, Kattelmann found that only 20% of the snowpack was wetted 12 hours after application of water to the surface, so that during the initial stages of infiltration the effective residual water content may be comparatively low. A tentative value of $s_r = 0.04$ is used in the model, which is subject to revision pending further study and analysis of field data.

The fluid flow model just presented assumes horizontal homogeneity in the snow cover. Seasonal snow covers that are undergoing freeze–thaw cycles or that are subject to strong winds develop crusts

* The evaporation term has been omitted here but will be included in the next version of the model.

and ice layers, which complicate the flow pattern. Perforations arise in the crusts through which fingers of water flow at a much faster rate than through the crust itself (Colbeck 1979). Field observations by Marsh and Woo (1984a) of runoff rates from ripe snow in the Canadian Arctic show that almost half the daily flow can be carried by fingers or flow channels that move ahead of the background front. The same authors have developed a simulation model that incorporates the phenomenon of fingering (Marsh and Woo 1984b). In addition to addressing the concerns of capillary flow at the water front and a more accurate determination of s_r, an enhanced version of the fluid flow model presented here should include the effects of fingering and of ponding above ice lenses.

Boundary conditions for mass and momentum balance

Mass fluxes of the three water phases across the air/snow interface consist of rainfall, snowfall and the turbulent exchange of water vapor. Velocities are taken with respect to the moving top boundary. In the case of snowfall or water ponding on a frozen or otherwise impermeable surface, mass flows result in a thickening of the top element by an amount

$$\frac{\partial \Delta z}{\partial t} = \frac{fallrate}{3600} - CR\,\Delta z \tag{47}$$

where the term CR is the compaction rate (eq 30), and *fallrate* represents hourly accumulation (m/hr). The mass precipitation flux U_p in kg/m^2 · s is given by

$$U_p = U^{n+1} = -\gamma_p \frac{fallrate}{3600} \tag{48}$$

where the precipitation density γ_p is 1000 kg/m^3 for rain, and from 20 to 200 kg/m^3 for snow, depending upon wind, crystal type and water content. For dry snow a representative value of 80 kg/m^3 is suggested. Accumulation is added in elemental increments of Δz_{inc}, which defaults to values of 4 cm for snow and 1 cm for ponding rain. At the beginning of a precipitation event, or when an element is full, the time step is automatically reduced to a minimum level, which is usually set at 5 s. In addition, Δt is constrained to be sufficiently small so that an element is not totally filled within one iteration. In the case of snowfall the top node is subdivided in a ratio of 1/3 to 2/3 once precipitation stops, subject to a minimum elemental thickness of 2 mm.

When substituted into eq 22–25, the mass balance equations for the top node n become

$$\frac{\partial}{\partial t}\left(\rho_t \Delta z\right) - \overline{\rho_{v,\,sat} f_{rh}}\,\frac{\partial\left(\theta_v \Delta z\right)}{\partial t} = -\left(\overline{U_p - U_\ell^n}\right) + \overline{\frac{E_{E0} + E_{Ew}}{L_{vk}}\left(P_{v,\,air} - f_{rh} P^n_{vk,\,sat}\right)} + \overline{U_v}^{\,n-\frac{1}{2}} \tag{49}$$

for the total media,

$$\frac{\partial}{\partial t}\left(\gamma_i \Delta z\right) = -\overline{\left(1 - f_{\ell p}\right) U_p} - \overline{M_{\ell i} \Delta z} - \overline{M_{vi}\,\Delta z}$$

for snowfall,

$$\frac{\partial}{\partial t}\left(\gamma_\ell\,\Delta z\right) = -\overline{f_{\ell p}\,U_p} + \overline{U_\ell^n} + \overline{M_{\ell i}\,\Delta z} - \overline{M_{v\ell}\,\Delta z}$$

for liquid water and

$$\overline{(\phi_{sd}-s\phi)\Delta z}\ \overline{f_{rh}C_{kT}}\frac{\partial T}{\partial t}=\overline{\frac{E_{E0}+E_E w}{L_{vk}}\left(P_{v,\,air}-f_{rh}P^{n}_{vk,\,sat}\right)}+\overline{U_v}^{\,n-\frac{1}{2}}+\overline{M_{vi}\,\Delta z}+\overline{M_{v\ell}\,\Delta z}$$

for water vapor, where

w = wind speed at a given height above the surface (m/s)
$P_{v,air}$ = water vapor pressure in air at a given height above the interface (mb)
$P_{vk,sat}$ = saturation water vapor pressure with respect to phase k (mb)
$f_{\ell p}$ = fractional mass liquid content of the precipitation
E_{E0} = windless exchange coefficient for latent heat (W/m^2·mb)
E_E = exchange coefficient for latent heat (J/mb · m^3)

and the exchange coefficients for latent heat are described later. The fluid flow equation for the top node is

$$\rho_\ell(1-s_r)\,\overline{\phi\Delta z}\frac{\partial s_e}{\partial t}=-\overline{f_{\ell p}U_p}-\frac{\rho_\ell^2 g}{\mu_\ell}\overline{\left(K_{max}\,s_e^3\right)}^{n}+\overline{M_{\ell i}\Delta z}\left(1-\frac{\rho_\ell}{\rho_i}\,\bar{s}\right)-\rho_\ell\,\bar{s}\,\frac{\partial\Delta z}{\partial t}\ . \qquad (50)$$

ENERGY BALANCE

Energy equation

Analogous to the conservation equations for mass and momentum, the conservation of energy stipulates that the time rate of change in stored energy within volume ΔV equals the net energy flux across the volume surface dS. The terminology "energy balance" in effect describes a "heat balance," since other sources of energy (such as macrokinetic, chemical and viscous dissipation) are of a lower order and are customarily discounted. The amount of heat associated with a unit of mass at temperature T relative to a reference level T_0 is expressed in terms of its specific enthalpy h_t (J/kg), which for an isobaric system is the heat required to raise or lower the temperature to T from T_0. If the fusion point of water (T = 273.15 K) is chosen for T_0, the general expression for specific enthalpy becomes

$$h=\int_{273.15}^{T}c(T)\,dT+L \qquad (51)$$

where c (J/kg·K) and L (J/kg) are the specific and latent heats, respectively. Neglecting sensible heat effects for the water vapor, the specific enthalpies for the constituents h_k are

$$\begin{aligned}h_i&=c_i(T-273.15)\\h_\ell&=c_\ell(T-273.15)+L_{\ell i}\\h_v&=L_{vi}\\h_d&=c_d(T-273.15).\end{aligned} \qquad (52)$$

Expressing the conductive flux by Fourier's law, where k_t is the thermal conductivity of the medium (W/m·K), and denoting the radiative flux as $\mathbf{I}_R$ (W/m^2), yields the following form of the energy equation:

$$\frac{\partial}{\partial t}\int_v \rho_t h_t\,dV=\overline{-\sum_k\int_S \mathbf{U}_k h_k\cdot d\mathbf{S}}+\overline{\int_S k_t\nabla\mathbf{T}\cdot d\mathbf{S}}+\overline{\int_S \mathbf{I}_R\cdot d\mathbf{S}} \qquad (53)$$

mass flux — conduction — radiative flux

where k = i, ℓ and v. The radiative flux here is defined as *positive downwards* and is the net of the downwelling and upwelling components. The first term on the right in eq 53 represents the transport of enthalpy through the mass flows of liquid water ($\mathbf{U}_\ell$), water vapor ($\mathbf{U}_v$) and falling dry snow or ice ($\mathbf{U}_i$), where the latter is constrained to the top node. Substituting eq 21 for the vapor flux and making the usual assumptions of vertical flow and nodal homogeneity, we can write eq 53 as

$$\underbrace{\frac{\partial}{\partial t}\left(\rho_t h_t \Delta z\right) - \overline{\rho_{vk,\,sat} f_{rh}} \frac{\partial\left(h_v \theta_v \Delta z\right)}{\partial t}}_{\text{rate of change in stored heat}} = \underbrace{-\overline{\left[\left(U_\ell h_\ell\right)^{j+1} - \left(U_\ell h_\ell\right)^{j}\right]}}_{\text{water flow}}$$

$$+ \underbrace{\overline{\left(h_v D_e C_{kT} \frac{\partial T}{\partial z}\right)^{j+\frac{1}{2}} - \left(h_v D_e C_{kT} \frac{\partial T}{\partial z}\right)^{j-\frac{1}{2}}}}_{\text{diffusive vapor flux}}$$

$$+ \underbrace{\overline{\left(k_t \frac{\partial T}{\partial z}\right)^{j+\frac{1}{2}} - \left(k_t \frac{\partial T}{\partial z}\right)^{j-\frac{1}{2}}}}_{\text{conduction}} + \underbrace{\overline{\left(I_s^{j+\frac{1}{2}} - I_s^{j-\frac{1}{2}}\right)}}_{\substack{\text{radiative} \\ \text{flux}}}. \tag{54}$$

As discussed later, it is assumed that only the short-wave radiation I_s penetrates beyond the top node. Air constitutes less that 1% of the total mass and, with the exception of the latent heat effects of water vapor, is omitted from the heat balance calculations. Together with the fluid flow and continuity equations (eq 46 and 22–25), the energy equation (eq 54) forms a closed set from which temperature, mass and phase changes may be computed.

Evaluation of eq 54 is facilitated by the use of bulk thermal properties to characterize the snow–soil mixture. Thus a combined specific heat c_t and combined specific enthalpy h_t for the total medium are defined in terms of the mass fractions γ_k/ρ_t of the constituent phases, as

$$c_t = \frac{1}{\rho_t} \sum_k \gamma_k c_k \approx \frac{1}{\rho_t} \left(\gamma_d c_d + \gamma_i c_i + \gamma_\ell c_\ell\right) \tag{55}$$

and

$$h_t = \frac{1}{\rho_t} \sum_k \left[\int_{273.15}^{T} \gamma_k c_k dT\right] + L_{\ell i} \frac{\gamma_\ell}{\rho_t} + L_{vi} \frac{\gamma_v}{\rho_t} \tag{56}$$

where k = i, ℓ and d

c_i = specific heat of ice (J/kg·K) = $-13.3 + 7.80\,T$ (K)

c_ℓ = specific heat of water (4217.7 J/kg·K)

c_d = specific heat of the dry soil (J/kg·K)

$L_{\ell i}$ = latent heat of fusion for ice (3.335×10^5 J/kg)

L_{vi} = latent heat of sublimation for ice (2.838×10^6 J/kg).

Employing the bulk enthalpy definition (eq 56), we can write the first term in eq 54 as

$$\frac{\partial}{\partial t}\left(\rho_t h_t \Delta z\right) = \frac{\partial}{\partial t}\left[\sum_k \int_{273.15}^{T} \gamma_k c_k \Delta z\, dT\right] + L_{\ell i} \frac{\partial\left(\gamma_\ell \Delta z\right)}{\partial t} + L_{vi} \frac{\partial\left(\gamma_v \Delta z\right)}{\partial t}. \tag{57}$$

Now expressing the bulk densities of ice and liquid water in terms of the unfrozen mass fraction f_ℓ as

$$\gamma_i = (1 - f_\ell)\,\gamma_w$$

and

$$\gamma_\ell = f_\ell\,\gamma_w \tag{58}$$

where $\gamma_w = \gamma_\ell + \gamma_i$, and differentiating under the integral, leads to the further simplification of

$$\frac{\partial}{\partial t}(\rho_t h_t \Delta z) = \overline{\rho_t c_t \Delta z}\,\frac{\partial T}{\partial t} + \frac{\partial}{\partial t}(\gamma_w \Delta z)\int_{273.15}^{\overline{T}} c_w\,dT + L_{\ell i}\frac{\partial(\gamma_\ell \Delta z)}{\partial t} + L_{vi}\frac{\partial(\gamma_v \Delta z)}{\partial t} \tag{59}$$

in which $c_w = f_\ell c_\ell + (1 - f_\ell)c_i$, and where the rate of change in water mass $[\partial(\gamma_w \Delta z)/\partial t]$ equals the net water flux (eq 23 and 24),* or

$$\frac{\partial}{\partial t}(\gamma_w \Delta z) = -\overline{\left(U_\ell^{j+1} - U_\ell^{j}\right)}\ . \tag{60}$$

If the bulk vapor density is expressed as $\gamma_v = f_{rh}\theta_v \rho_{v,sat}$, the term $\partial(\gamma_v \Delta z)/\partial t$ in eq 59 can be specified in terms of the variation in saturation vapor density with temperature (C_{kT}) and the volume fraction ($\theta_v = \phi_{sd} - s\phi$) as

$$\frac{\partial}{\partial t}(\gamma_v \Delta z) = \frac{\partial}{\partial t}(f_{rh}\,\theta_v\,\rho_{vk,\,sat}\Delta z) = \overline{\rho_{v,sat}\,f_{rh}}\,\frac{\partial \theta_v \Delta z}{\partial t} + \overline{(\phi_{sd} - s\phi)\Delta z}\;\overline{f_{rh}\,C_{kT}}\,\frac{\partial T}{\partial t}\ . \tag{61}$$

Now using eq 59–61 and substituting the enthalpy expressions into the flux terms, we can write eq 54 as

$$\left[\overline{\rho_t c_t \Delta z} + L_{vi}\,\overline{(\phi_{sd} - s\phi)\Delta z}\;\overline{f_{rh}\,C_{kT}}\right]\frac{\partial T}{\partial t} - \overline{\left(U_\ell^{j+1} - U_\ell^{j}\right)}\left[\int_{273.15}^{T} c_w\,dT + c_\ell\,273.15 - L_{\ell i}\right]$$

$$+ L_{\ell i}\frac{\partial \gamma_\ell \Delta z}{\partial t} = -c_\ell\overline{\left[(U_\ell T_\ell)^{j+1} - (U_\ell T_\ell)^{j}\right]} + \overline{\left(k_e\frac{\partial T}{\partial z}\right)^{j+\frac{1}{2}} - \left(k_e\frac{\partial T}{\partial z}\right)^{j-\frac{1}{2}}} + \overline{\left(I_s^{\,j+\frac{1}{2}} - I_s^{\,j-\frac{1}{2}}\right)} \tag{62}$$

where k = i if $\theta_\ell \le 0.02$ and k = ℓ if $\theta_\ell > 0.02$. Heat transport through conduction and vapor diffusion have been combined through use of an effective thermal conductivity, $k_e \equiv k_t + L_{vi}D_e C_{kT}$ (W/K · m), in which the thermal conductivity of soil is computed from the algorithm of Johansen (as reported by Farouki 1981), and the thermal conductivity of snow k_s is estimated as

$$k_s = k_a + \left(7.75 \times 10^{-5}\,\gamma_s + 1.105 \times 10^{-6}\,\gamma_s^2\right)(k_i - k_a)\,. \tag{63}$$

In this relationship the conductivities of air k_a and ice k_i are 0.023 and 2.29 W/K · m, respectively, and the adjustable parameters have been selected so that k_e fits the data of Yen (1962) and extrapolates to k_i when the snow density is that of ice.

---

* Exchange with the vapor phase is omitted, since sensible heat effects for this phase have been neglected.

Latent heat changes resulting from additional liquid water in the mix, either through water flow or freeze–thaw of the snow cover, are included in the term $L_{\ell i}\partial\gamma_\ell\Delta z/\partial t$ of the heat balance equation (eq 62). Solution of the equation requires further specification of this term, which will be addressed in the next section. Alternative derivations of the energy equation for porous media can be found in the work of Morland et al. (1990), Lunardini (1988) and Morris (1987).

Phase change

The nodal heat balance equations each contain four unknowns: the latent heat change, $L_{\ell i}\partial\gamma_\ell\Delta z/\partial t$, and temperatures for the node and its first neighbors. In the case of snow, since the transition between solid and liquid phases occurs sharply near 0°C, we could proceed with two independent solutions for the heat equation. First the temperature profiles are calculated, where the temperature is held at 0°C for nodes undergoing phase change, and then the amount of melt is computed (Morris 1987). Alternatively we could use the apparent heat capacity method described by Albert (1983). In this procedure, total enthalpy changes (both latent and sensible) are expressed in terms of temperature through the definition of an apparent specific heat c_{app}, such that

$$\Delta h_t = c_{app}\,\Delta t \ . \tag{64}$$

For substances with abrupt phase boundaries, latent heat changes are artificially allowed to occur over a small temperature interval δT about the fusion point, leading to a definition of c_{app} as

$$c_{app} = c + \frac{L_{\ell i}}{\delta T} \ . \tag{65}$$

Within a porous medium, a fraction of unfrozen water f_ℓ coexists in equilibrium with ice at temperatures below 0°C. Thus, for porous media the apparent heat capacity method has a physical basis and is the preferred numerical approach.

If hysteresis effects are disregarded, the unfrozen water content within a given medium is a single-valued function of temperature and has a freezing curve characteristic of the snow–soil properties. In the absence of water flow, the change in the mass fraction of liquid water is then directly related to phase change, and the apparent specific heat can be written in terms of the slope of the freezing curve as

$$c_{app} = c_t + \frac{\gamma_w}{\rho_t} L_{\ell i} \frac{\partial f_\ell}{\partial T} \ . \tag{66}$$

This means of defining the apparent specific heat was adopted by Guryanov (1985), who proposed the following semi-empirical function for f_ℓ:

$$f_\ell = \frac{\gamma_\ell}{\gamma_w} = \frac{1 - 0.75\,\frac{\gamma_d}{\gamma_w} J_p}{1 + (a1\,T_D)^2} + \frac{0.75\,\frac{\gamma_d}{\gamma_w} J_p}{1 + (a2\,T_D)^{4/3}} \tag{67}$$

where J_p = plasticity index (fraction of water)
$a1 = 0.2/(0.01 + J_p)$
$a2 = 0.01/(0.1 + J_p)$
T_D = depression temperature (K), defined as $273.15 - T$.

Although less complex functions for unfrozen water content are in frequent use (Tice et al. 1976), the Guryanov model has the advantage of being continuous at $T = 0$°C. The two terms in eq 67 correspond to free (or capillary) and bound (or hygroscopic) water. The capillary term dominates at temperatures near 0°C but diminishes rapidly with depression temperature. Associated with hygroscopic water is

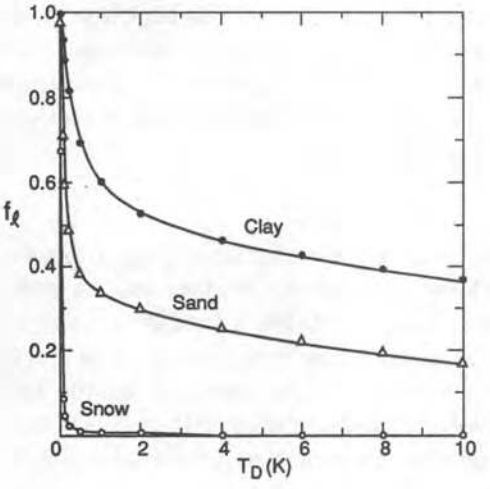

Figure 3. Mass liquid water fraction f_ℓ predicted by eq 67. The equation parameters are:

Snow	$a1 = 100$
Sand	$J_p = 0.02$
	Gravimetric water content $(\gamma_w/\gamma_d) = 0.05$
Clay	$J_p = 0.15$
	Gravimetric water content $(\gamma_w/\gamma_d) = 0.25$

a minimum unfrozen level for a given depression temperature. In order that eq 67 be well behaved, a minimum water content is set at $0.75\,\gamma_d J_p$. The plasticity index J_p ranges from 0.0 for coarse soils, such as gravel or sand, to greater than 0.15 for fine-grained clays. The plasticity index for snow is 0, and a value of 100 is arbitrarily selected for $a1$. The resulting curve approaches a step function, in which 99% of the water is frozen at a depression temperatures of 0.10°C. Curves calculated from eq 67 for snow, sand (J_p= 0.02) and clay (J_p= 0.15) are shown in Figure 3.

The term F is introduced to denote the slope of the freezing curve ($\partial f_\ell/\partial T$), which is found by differentiation of eq 67:

$$F \equiv \frac{\partial f_\ell}{\partial T} = \frac{2\,T_D a1^2\left(1-0.75\,\frac{\gamma_d}{\gamma_w}J_p\right)}{\left[1+(a1\,T_D)^2\right]^2} + \frac{a2\,\frac{4}{3}\,T_D^{\frac{1}{3}}\,\frac{\gamma_d}{\gamma_w}J_p}{\left[1+(a2\,T_D)^{\frac{4}{3}}\right]^2}\,. \tag{68}$$

Substituting F into eq 66 provides a function for the apparent specific heat. In general, there is an immediate rise in c_{app} as freezing commences, followed by an exponential drop as temperatures fall below 0°C.

Changes in the latent heat component of enthalpy result both from phase change and from the influx of other phases. Applying the chain rule to the expression $L_{\ell i}\partial\gamma_\ell\Delta z/\partial t$ in eq 62, and substituting F for $\partial f_\ell/\partial T$, gives an expression for latent heat changes in liquid water:

$$\frac{L_{\ell i}\,\partial\left(\gamma_\ell\,\Delta z\right)}{\partial t} = \frac{L_{\ell i}\,\partial\left(f_\ell\gamma_w\Delta z\right)}{\partial t} = L_{\ell i}\left(\overline{\gamma_w\Delta z}\;\overline{F}\;\frac{\partial T}{\partial t} + \bar{f}_\ell\,\frac{\partial\gamma_w\Delta z}{\partial t}\right). \tag{69}$$

Expressing the change in mass density $\partial\gamma_w\Delta z/\partial t$ in terms of the net water flux (eq 60) gives

$$\frac{L_{\ell i}\,\partial\left(\gamma_\ell\Delta z\right)}{\partial t} = L_{\ell i}\,\overline{\gamma_w\Delta z}\;\overline{F}\,\frac{\partial T}{\partial t} - \bar{f}_\ell L_{\ell i}\left(\overline{U_\ell^{j+1}-U_\ell^{j}}\right). \tag{70}$$

latent heat change — freeze–thaw of medium — unfrozen net flux

Using the definition of f_ℓ (eq 67), the function $\int c_w dT$ in eq 62 can be integrated to give

$$\int_{273.15}^{T}\left[c_i\left(1-f_\ell\right)+c_\ell f_\ell\right]dT = c_i(T-273.15) - \left(c_\ell - c_i\right)\left\{\frac{\tan^{-1}\left(a1\,T_D\right)}{a1}\left(1-0.75\,\frac{\gamma_d}{\gamma_w}J_p\right)\right.$$

$$+\frac{0.5625}{\sqrt{2}\,a2}\,\frac{\gamma_d}{\gamma_w}\,J_p\cdot\left[\ln\left(\frac{(a2T_D)^{2/3}-\sqrt{2}\,(a2T_D)^{1/3}+1}{(a2T_D)^{2/3}+\sqrt{2}\,(a2T_D)^{1/3}+1}\right)+2\,\tan^{-1}\left(\frac{\sqrt{2}\,(a2T_D)^{1/3}}{1-(a2T_D)^{2/3}}\right)\right]\right\}. \quad (71)$$

For the case of snow, where $a1$ is very large and J_p is zero, it is reasonable to simplify eq 71 to $c_i(T-273.15)$. Now an enthalpy adjustment factor H is defined as

$$H \equiv \int_{273.15}^{T}\left[c_i\left(1-f_\ell\right)+c_\ell f_\ell\right]dT + c_\ell\,273.15 \quad (72)$$

which becomes

$$H \equiv c_i T + \left(c_\ell - c_i\right)273.15$$

for snow,

$$H \equiv c_\ell T$$

for unfrozen soil and

$$H \equiv c_i T + \left(c_\ell - c_i\right)273.15 - \left(c_\ell - c_i\right)\left\{\frac{\tan^{-1}(a1\,T_D)}{a1}\left(1-0.75\,\frac{\gamma_d}{\gamma_w}J_p\right)\right.$$

$$\left.+\frac{0.5625}{\sqrt{2}\,a2}\,\frac{\gamma_d}{\gamma_w}\,J_p\cdot\left[\ln\left(\frac{(a2T_D)^{2/3}-\sqrt{2}\,(a2T_D)^{1/3}+1}{(a2T_D)^{2/3}+\sqrt{2}\,(a2T_D)^{1/3}+1}\right)+2\,\tan^{-1}\left(\frac{\sqrt{2}\,(a2T_D)^{1/3}}{1-(a2T_D)^{2/3}}\right)\right]\right\} \quad (73)$$

for frozen soil.

Using eq 70–73, we can simplify eq 62:

$$\left[\overline{\rho_t c_t \Delta z}+L_{\ell i}\,\overline{\gamma_w \Delta z}\;\overline{F}+L_{vi}\,\overline{\left(\phi_{sd}-s\phi\right)\Delta z}\;\overline{f_{rh}C_{kT}}\right]\frac{\partial T}{\partial t}-\left(\overline{U_\ell^{j+1}-U_\ell^{j}}\right)\left[\overline{H}-L_{\ell i}\left(1-\overline{f_\ell}\right)\right]$$

$$=-c_\ell\left[\overline{(U_\ell T_\ell)^{j+1}-(U_\ell T_\ell)^{j}}\right]+\overline{\left(k_e\frac{\partial T}{\partial z}\right)^{j+\frac{1}{2}}-\left(k_e\frac{\partial T}{\partial z}\right)^{j-\frac{1}{2}}}+\overline{\left(I_s^{j+\frac{1}{2}}-I_s^{j-\frac{1}{2}}\right)} \quad (74)$$

which is the final form of the heat balance equation. The second term on the left accounts for the heat gained through freezing of an infiltrating water flux. Note that for unfrozen soil ($f_\ell = 1$), it is canceled by a portion of the water flow term on the right, which then reduces to $-c_\ell\overline{U}_\ell^{j}\left(T^{j+\frac{1}{2}}-T^{j-\frac{1}{2}}\right)$ when a central difference scheme is used. The latter expression is the more standard representation of the water flow term in coupled mass and energy balance equations. The heat flow problem is solved numerically through a system of equations, one for each node, subject to a meteorologically determined heat flux across the air interface and to a constant temperature at the bottom boundary.

Surface energy balance

The surface energy balance I_{top} at the air interface is composed of the turbulent fluxes of sensible and latent heat, the short- and long-wave components of radiation, and convected heat due to snow or rainfall. Mathematically this takes the form

$$I_{top} = I_s\downarrow(1 - \alpha_{top}) + I_{ir}\downarrow - I_{ir}\uparrow + I_{sen} + I_{lat} + I_{conv} \tag{75}$$

where $I_s\downarrow$ = energy flux of downwelling short-wave radiation (W/m^2)
α_{top} = albedo or short-wave reflectance (W/m^2)
$I_{ir}\downarrow$ = energy flux of downwelling long-wave radiation (W/m^2)
$I_{ir}\uparrow$ = energy flux of upwelling long-wave radiation (W/m^2)
I_{sen} = turbulent flux of sensible heat (W/m^2)
I_{lat} = turbulent flux of latent heat (W/m^2)
I_{conv} = heat convected by rain or falling snow (W/m^2).

Contrary to the usual convention employed throughout this report, the surface fluxes are defined as *positive downwards*. The magnitude of turbulent exchange primarily depends on surface roughness, wind speed and the atmospheric gradients of temperature and humidity. Radiation incident on the earth's surface is composed of emissions from the sun and the earth's atmosphere. The spectrum is divided accordingly into solar or short-wave (0.3–3 μm) and terrestrial or long-wave (3–100 μm) components.* The portion of incident radiation to be either absorbed or re-emitted back into the atmosphere varies both with wavelength and with the optical properties of the medium and is parameterized in terms of albedo for short-wave radiation and emissivity for long-wave radiation.

Solar heating

As a first approximation the solar energy incident on the snow cover is assumed to be diffuse and isotropic. Radiation entering the snow cover is subdivided into near-infrared and visible components, with corresponding bulk extinction coefficients β_{nir} and $\beta_{vis.}$ For β_{vis} the asymptotic bulk extinction coefficient β_∞ is used, which is represented by the function of Bohren and Barkstrom (1974) as

$$\beta_{vis} \approx \beta_\infty = \frac{0.003795\ \gamma_w}{\sqrt{d}} \tag{76}$$

where the adjustable parameter is taken from Anderson (1976). Extinction of near-infrared radiation is constrained to the top node and assumes an elemental thickness of 2 mm. The value for β_{nir} is input to the program. Combining these effects, the energy gain due to solar heating Q_{solar} within the snow cover is estimated as

$$Q^n_{solar} \equiv I_s^{n+\frac{1}{2}} - I_s^{n-\frac{1}{2}} = I_s\downarrow(1 - \alpha_{top})\left(1 - e^{-\beta_\infty \Delta z}\ e^{-\beta_{nir} 0.002}\right)^n$$

for the top element and

$$Q^j_{solar} \equiv I_s^{j+\frac{1}{2}} - I_s^{j-\frac{1}{2}} = I_s^{j+\frac{1}{2}}\left(1 - e^{-\beta_\infty \Delta z}\right)^j \tag{77}$$

for the interior elements, where

$$I_s^{j+\frac{1}{2}} = I_s\downarrow(1 - \alpha_{top}) - \sum_{i=j+1}^{n} Q^i_{solar}\ .$$

The albedos for both snow and soil are input as constant parameters, with default values of 0.78 and 0.40, respectively.

---

* The wavelength cut-off between short- and long-wave radiation is somewhat arbitrary. A value of 3 μm was selected here because it corresponds to the spectral limits of the Eppley radiometers, which were used for the radiation measurements.

Estimation of short-wave radiation

Incident short-wave or solar radiation is composed of direct and diffuse components, the latter being scattered during its passage through the atmosphere. Diffuse radiation is largely isotropic, although the intensity is higher beneath the portion of the sky dome nearest the sun. Incident and reflected solar fluxes are customarily measured with hemispherically averaging radiometers, the net of which is used directly in the energy equation. As a default measure the incident solar flux is estimated from the two-stream model of Shapiro (1982, 1987). A brief description of his procedure follows.

In Shapiro's model the atmosphere is subdivided into N horizontally infinite plane–parallel layers. Following the two-stream formulation for a thin atmosphere, the angular distribution is simplified into bidirectional forward and backward components. Shapiro defines a reflectivity $\mathcal{R}$ and apparent transmissivity $\mathcal{T}$ for each layer, in which $\mathcal{R}$ is analogous to the backscatter, and according to conservation of energy, $\mathcal{T}$ is given by

$$\mathcal{T} = 1 - \mathcal{R} - \mathcal{A} \tag{78}$$

where $\mathcal{A}$ is the absorptivity. Note that by this definition $\mathcal{T}$ includes both unscattered and forward scattered radiation. The radiative transfer equations are then given by

$$I_s^{j''-\frac{1}{2}}\downarrow = \mathcal{T}_{j''} I_s^{j''+\frac{1}{2}}\downarrow + \mathcal{R}_{j''} I_s^{j''-\frac{1}{2}}\uparrow$$

$$I_s^{j''+\frac{1}{2}}\uparrow = \mathcal{T}_{j''} I_s^{j''-\frac{1}{2}}\uparrow + \mathcal{R}_{j''} I_s^{j''+\frac{1}{2}}\downarrow \tag{79}$$

where the index j'' numbers in ascending order from the air interface. Using curve fits to large amounts of data from the SOLMET data base, Shapiro has tabulated values for $\mathcal{R}_{j''}$ and $\mathcal{T}_{j''}$ as polynomial functions of the solar zenith angle θ_z and cloud conditions. Specifying the upper and lower boundary conditions as

$$I_s^{N+\frac{1}{2}} = I_{s00}$$

and

$$I_s^{\frac{1}{2}}\uparrow = \mathcal{R}_0 I_s^{\frac{1}{2}}\downarrow = \alpha_{top} I_s^{\frac{1}{2}}\downarrow \tag{80}$$

where I_{s00} is the solar insolation at the top of the atmosphere, leads to a system of $2N + 2$ linear equations, which can be solved for the incident flux $I_s^{\frac{1}{2}}\downarrow$ at the earth's surface. In addition to the N-level model, Shapiro has proposed a simplified three-level algorithm with layers corresponding to heights of low ($j'' = 1$), midlevel ($j'' = 2$) and high ($j'' = 3$) clouds, as shown in Figure 4.* Equation set 79 is then solved in closed form to obtain

$$I_s\downarrow(Z) = I_s^{\frac{1}{2}}\downarrow = \frac{\mathcal{T}_1\mathcal{T}_2\mathcal{T}_3}{D_2} I_{s00} \tag{81}$$

where

$$D_2 = d_1\left(d_3 d_2 - \mathcal{R}_3\mathcal{R}_1\mathcal{T}_2^2\right) - d_3\,\mathcal{R}_2\alpha_{top}\mathcal{T}_1^2 - \mathcal{R}_3\alpha_{top}\left(\mathcal{T}_2\mathcal{T}_1\right)^2 \tag{82}$$

* The indexing here is the reverse of that used by Shapiro, who uses values of $j'' = 1, 2$ and 3 for high, middle and low clouds, respectively.

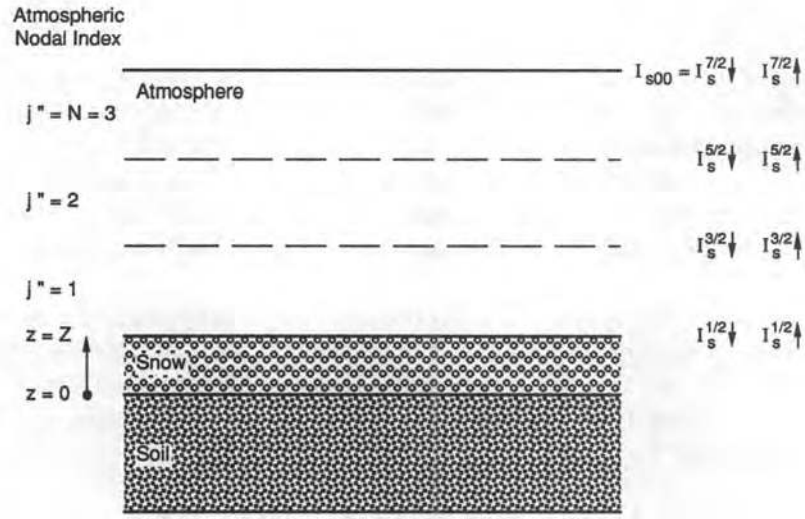

Figure 4. Conceptual geometry for a three-layer solar insolation model.

and the coefficients $d_{j''}$ are defined as

$$d_j'' \equiv 1 - \mathcal{R}_j'' \mathcal{R}_{j''-1} \cdot \tag{83}$$

Direct radiation is taken as that which is transmitted to the earth unscattered by the atmosphere. As a first approximation the transmissivity $\mathcal{T}d$ is computed by assuming that radiation is scattered isotropically, so that the backward and forward components are equal. In this case $\mathcal{T}d = \mathcal{T} - \mathcal{R}$ and the direct radiation incident on the earth is

$$I_{s,\,direct}\downarrow(Z) = \mathcal{T}d_1\,\mathcal{T}d_2\,\mathcal{T}d_3\,I_{s00} \tag{84}$$

and diffuse radiation is the complement of this, or

$$I_{s,diffuse}\downarrow(Z) = I_s\downarrow(Z) - I_{s,direct}\downarrow(Z) \tag{85}$$

where the position of the snow surface relative to the ground is denoted by the snow depth Z.*

Adjustment of solar radiation for sloped surfaces.

In the appendix to his report, Shapiro (1987) included an adjustment for radiation incident on a sloped surface. His algorithm takes into account reflected radiation from the horizontal plane and changes in diffuse radiation due to varying exposure of the slope to the solar and antisolar quadraspheres, as well as the standard correction for the intensity of direct radiation. The slope is characterized by an upslope vector in the direction of greatest ascent, where the elevation angle e (radians) is measured between the vector and its horizontal projection, and the azimuthal or aspect angle ϕ_{asp} (radians) is measured clockwise from north to the horizontal projection, as shown in Figure 5. The position of the sun is specified by the solar zenith angle θ_z and the azimuthal angle ϕ_{solar},

* The computer routines for estimating both solar and long-wave radiation have been adapted from the codes of Glen Higgins and Joan-Marie Freni of Systems and Applied Sciences Corporation, under contract to the Air Force Geophysics Laboratory.

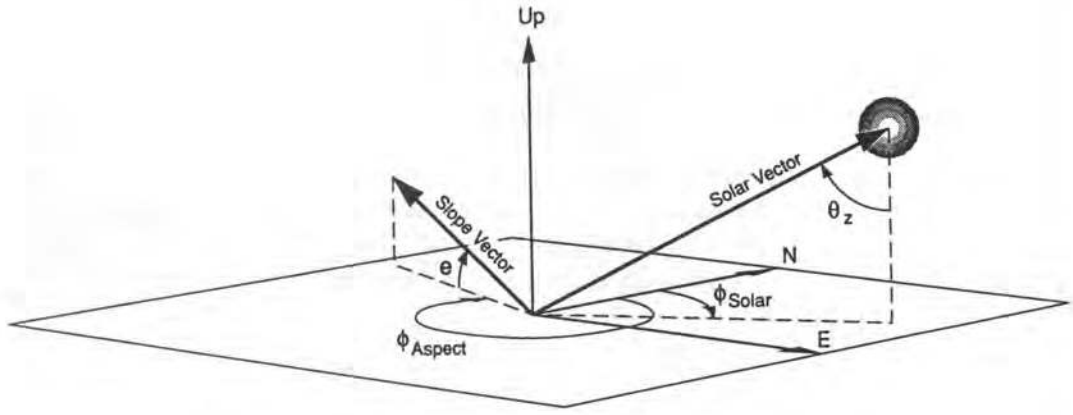

Figure 5. Geometry for radiation incident on a sloped surface.

measured clockwise from north to the horizontal projection of the solar position vector. Under clear skies the adjusted radiation for a slope of given elevation and aspect angle is

$$I_{s,slope}\downarrow = I_{s,direct}\downarrow\left[\cos e + \frac{\sin\theta_z \sin e \cos\Delta\phi_{asp}}{\cos\theta_z}\right]$$

$$+ I_{s,diffuse}\downarrow\frac{(\pi-\Delta\phi_{asp})(S+\cos e)+\Delta\phi_{asp}(1+S\cos e)}{\pi(1+S)} + I_s\downarrow\frac{\alpha_{top}(1-\cos e)}{2} \qquad (86)$$

where the latter term accounts for reflected radiation, $\Delta\phi_{asp}$ is the aspect angle relative to the azimuthal angle of the sun, and S is the ratio of the average diffuse radiance from the solar and anti-solar quadraspheres, computed as

$$S \equiv 1 + 0.5\sin\theta_z + 2.0\sin 2\theta_z \qquad (87)$$

By convention $\Delta\phi_{asp}$ is defined as zero for a south-facing slope, giving $\Delta\phi_{asp} \equiv \left|\left|\phi_{asp} - \phi_{solar}\right| - \pi\right|$. A further correction is included in the code for diffuse radiation under cloudy skies.

Long-wave radiation

All materials radiate electromagnetic energy, the intensity being a function of their temperature and surface characteristics. The power spectrum emitted by a black body, or perfect absorber, is known as Planck's law and is written as

$$I_{emit}(\lambda) = \frac{2\pi c8\lambda^{-5}}{e^{\frac{c9}{\lambda T}} - 1} \qquad (88)$$

where $I_{emit}(\lambda)$ = intensity of hemispherically emitted radiation of wavelength λ (W/m^3)
T = absolute temperature (K)
$c8 = 0.59544 \times 10^{-16}\ Wm^2$
$c9 = 1.4388 \times 10^{-2}$ Km (Siegal and Howell 1972, p. 19 and 738).

The emissivity ε of a specified material is the ratio of its emitted energy to that of a black body at the same temperature. Integrating Planck's law over the power spectrum gives the well-known Stefan–Boltzmann expression for the all-wave hemispherical emitted intensity I_{emit}:

$$I_{\text{emit}} = \varepsilon\sigma T^4 \tag{89}$$

where σ is the Stefan–Boltzmann constant (5.669×10^{-8} W/m$^2 \cdot$ K^4).

The net long-wave exchange consists of upwelling thermal emissions from the earth's surface and downwelling emissions from gases and particulate matter in the atmosphere. Generally speaking, the earth radiates as a gray body and the power spectrum has the form of Planck's law. The upwelling long-wave flux $I_{\text{ir}}\uparrow$ in the boundary equation (eq 75) therefore contains an emitted component, which corresponds to the Stefan–Boltzmann equation, and a reflected component, which is proportional to the downwelling flux. In accordance with Kirchoff's Law, the emissivity and reflectance must sum to 1.0, so that

$$I_{\text{ir}}\uparrow = \varepsilon\sigma T^4 + (1 - \varepsilon) I_{\text{ir}}\downarrow. \tag{90}$$

Although eq 90 is customarily regarded as a boundary condition, infrared radiation penetrates the snow cover to 5–8 mm. The present minimum thickness of 2 mm will therefore be increased in subsequent versions of the code, so that most infrared radiation is absorbed within the top element. Snow is nearly a black body, with an emissivity approaching 1.0 (Warren 1982). Based on a comparison of measured radiation with estimates from the Stefan–Boltzmann Law, a value of 0.97 is suggested for the emissivity (Jordan et al. 1989).

Estimation of downwelling long-wave radiation

The downwelling long-wave flux under clear skies is estimated using the formula of Idso (1981), which is referred to in the literature as Idso2 and has the form

$$I_{\text{ir, clear}}\downarrow = \sigma\varepsilon_{\text{air}} T_{\text{air}}^4 = \sigma\left[0.70 + 5.95 \times 10^{-5} P_{\text{v, air}}\, e^{\frac{1500}{T_{\text{air}}}}\right] T_{\text{air}}^4 \tag{91}$$

where ε_{air} = clear-air all-wave bulk emissivity of the atmosphere
$P_{\text{v,air}}$ = water vapor pressure at a reference height above the surface (mb)
T_{air} = air temperature at a reference height above the surface (K).

The Idso formula tends to overestimate the emissivity and is therefore adjusted using the Wachtmann correction (Hodges et al. 1983):

$$\varepsilon'_{\text{air}} = -0.792 + 3.161\ \varepsilon_{\text{air}} - 1.573\ \varepsilon_{\text{air}}^2 \tag{92}$$

where $\varepsilon'_{\text{air}}$ is the corrected emissivity. An additional downwelling long-wave component is computed in the code for the emittance from clouds. No correction has been included for sloped surfaces, which will see less of the sky dome but will additionally receive a diffuse component from adjacent terrain.

Models of the Idso type, which estimate atmospheric emissivity from surface values of air temperature and water pressure, are good general indicators of long-wave radiation but are often of insufficient accuracy for energy balance computations (Jordan et al. 1989). Further modifications in the procedure are needed, particularly for the case of atmospheric inversions, which occur frequently over snow.

Turbulent exchange

The turbulent fluxes of latent and sensible heat are defined as (Andreas and Murphy 1986)*

---

* In this version of SNTHERM the latent heat flux is defined in terms of vapor pressure. Subsequent versions use the more standard parameter of vapor density.

$$I_{sen} = \left(E_{H0} + \rho_{air} c_{air} C_H w\right)\left(T_{air} - T^n\right) = \left(E_{H0} + E_H w\right)\left(T_{air} - T^n\right) \tag{93}$$

$$I_{lat} = \left(E_{E0} + \frac{100 L_{vi}}{R_w T_{air}} C_E w\right)\left(P_{v,\,air} - f_{rh} P^n_{vk,\,sat}\right) = \left(E_{E0} + E_E w\right)\left(P_{v,\,air} - f_{rh} P^n_{vk,\,sat}\right)$$

where ρ_{air} = air density (kg/m^3)
c_{air} = specific heat of air at constant pressure (J/kg·K)
T^n = surface temperature, approximated by that of the top node (K)
C_H = bulk transfer coefficient for sensible heat (dimensionless)
C_E = bulk transfer coefficient for latent heat (dimensionless)

and the fluxes are defined as *positive downwards*. Within a snow cover, water vapor is assumed to be at saturation and $f_{rh} = 1.0$. Vapor pressure is computed using the procedure of Buck (1981) and can optionally be taken as relative to ice or water. The exchange coefficients E_H (J/K · m^3) and E_E (J/mb· m^3) are related to the bulk transfer coefficients as

$$E_H = \rho_{air} c_{air} C_H$$

and

$$E_E = \frac{100 L_{vk}}{R_w T_{air}} C_E \tag{94}$$

The parameters $E_{H0} = 2.0 \pm 0.5$ W/m^2·K and $E_{E0} = 2.00 \pm 0.5$ W/m^2 · mb in eq 93 are windless convection coefficients for exchange over snow and are determined empirically. They are larger in magnitude than would be theoretically predicted by the limiting case of molecular diffusion, and they indicate the need for further study of windless exchange above snow. Bulk transfer coefficients are defined in terms of the roughness length z_0 for velocity and the measurement reference heights Z'_W, Z'_T and Z'_Q for wind speed, temperature and relative humidity, as

$$C_D = \frac{k^2}{\left[\varnothing_M \ln\left(\frac{Z'_W}{z_0}\right)\right]^2} \qquad C_E = \frac{C_{DN}}{\varnothing_M \varnothing_E \left[Sc_N + \frac{\ln\left(\frac{Z'_Q}{Z'_W}\right)}{\ln\left(\frac{Z'_W}{z_0}\right)}\right]}$$

$$C_H = \frac{C_{DN}}{\varnothing_M \varnothing_H \left[Pr_N + \frac{\ln\left(\frac{Z'_T}{Z'_W}\right)}{\ln\left(\frac{Z'_W}{z_0}\right)}\right]} \tag{95}$$

Errata: The ratios C_{DN}/C_{HN} and C_{DN}/C_{EN} should not be designated as the turbulent Prandtl and Schmidt numbers, the latter being defined as the ratios of the eddy transfer coefficients. In subsequent versions of the model the stability functions have been replaced with the flux-profile (Ψ) formulas. The upgraded procedures are documented in the Technical Note *Estimating the Turbulent Transfer Functions for Use in Energy Balance Models*, which is available from the author.

where C_D is the drag coefficient (dimensionless), k is the von Karman's constant (0.40), Sc_N and Pr_N are the turbulent Schmidt and Prandtl numbers, defined for neutral stability and at the measurement height for wind speed, as

$$Sc_N = \frac{C_{DN}\left(Z_Q' = Z_W'\right)}{C_{EN}}$$

$$Pr_N = \frac{C_{DN}\left(Z_T' = Z_W'\right)}{C_{HN}} \tag{96}$$

where $\varnothing$ represents the stability functions defined as (Anderson 1976)

$$\varnothing_M = \varnothing_E = \varnothing_H = 1 \tag{97a}$$

for neutral stability ($Ri = 0.00$),

$$\varnothing_M = \varnothing_E = \varnothing_H = \frac{1}{1 - 5Ri} \tag{97b}$$

for stable conditions when $0.00 < Ri < 0.20$,

$$\frac{1}{\varnothing_M} = \frac{1}{\varnothing_E} = \frac{1}{\varnothing_H} = 0 \tag{97c}$$

for stable conditions when $Ri \geq 0.20$ and

$$\varnothing_M = \frac{1}{(1 - 16Ri)^{0.25}}$$

$$\varnothing_H = \varnothing_E = \frac{1}{(1 - 16Ri)^{0.5}} \tag{97d}$$

for unstable conditions ($Ri < 0.00$). C_{DN}, C_{EN} and C_{HN} are the bulk transfer coefficients at neutral stability. The bulk Richardson number Ri is estimated as

$$Ri \approx \frac{gZ'\left(T_{air} - T^n\right)}{0.5\left(T_{air} + T^n\right)w^2} \tag{98}$$

where g is the acceleration due to gravity. The use of these stability functions over snow for the stable case consistently underpredicted the convective exchange and markedly degraded the predictive ability of the model. Therefore, as a temporary measure, the stability correction is not used for snow under stable atmospheric conditions.

On the basis of the best fit for surface temperature predictions, a roughness length of 2 ±1 mm is suggested for snow, which yields a drag coefficient C_{DN} of 3.35×10^{-3} under neutral stability at a measurement reference height of 2.0 m. Measurements used in validating the model were made with thermocouples, which were subject to solar loading and were not always in thermal contact with the snow cover, so this is not an exact figure. Values of 0.7 and 1.0 are suggested for the turbulent Prandtl

and Schmidt numbers, respectively. On theoretical grounds there is no justification for setting Sc_N to 1.0, but the use of a lower value resulted in unrealistically high latent heat losses in cases of moderate to high winds. The problem may lie in the assumption that water vapor is at saturation at the surface, which is probably not true during windy periods. Using values of 1005.0 J/kg·K, 1.276 kg/m^3 and 2.838×10^6 for c_{air}, ρ_{air} (at 0°C and 1000 mb) and L_{vi}, respectively, and reference heights of 2 m for Z_T' and Z_Q', the exchange coefficients at neutral stability evaluate to $E_H = 6.14$ J/K·m^3 and $E_E = 7.55$ J/mb·m^3.

The exchange coefficient for latent heat can be measured directly by noting the amount of evaporation from pans of snow inserted so that they are flush with the top of the snow cover. Determinations of E_E by this procedure as reported in the literature ranged from 4.82 to 10.78 (Anderson 1976, Table 2.1, for a reference height of 2 m). For wind speeds from 0.5 to 5.5 m/s, Anderson (Fig. 5.4) computed a value of 7.8 for E_E. The empirical value of 7.55 used in this study is correspondingly in the midrange of wind functions determined by evaporation. On the other hand, values in the literature for z_0 over snow ranged from 0.1 to 2.3 mm (Anderson 1976) and are therefore mostly lower than the value of 2 mm used here, although Dunne et al. (1976) assumed values of z_0 = 5 and 15 mm in computing runoff from a melting snow cover. Andreas (1987) reported $C_{HN} = 0.9 \pm 0.3 \times 10^{-3}$ and $C_{EN} = 2.5 \pm 0.5 \times 10^{-3}$ for measurements made by Hicks and Martin (1972), and C_{HN} = 1.1–1.5 $\times 10^{-3}$ for measurements made by Kondo and Yamazawa (1986), both of which again suggest that a value of 3.35×10^{-3} for C_{DN} may be too high.

Consistent with the stipulation that air is at rest within the pore space, it is assumed that turbulent energy dissipates abruptly at the surface. Although this boundary condition is customarily applied in heat-budget modeling, in reality a degree of wind penetration occurs within an open material such as snow. The usual assumptions of thermal equilibrium and stagnant air are made for this study, but a revised formulation is indicated for the future.

Energy equation for the top node

Combining eq 77, 90 and 93, and using the definitions for the precipitation flux given earlier, we can express the top energy flux (eq 75) as

$$I_{top} = I_s\downarrow(1 - \alpha_{top}) + \varepsilon I_{ir}\downarrow - \sigma\varepsilon(T^n)^4 + (E_{H0} + E_{Hw})(T_{air} - T^n) + (E_{E0} + E_{Ew})(P_{v,\,air} - f_{rh} P^n_{vk,\,sat}) - c_p U_p T_p \qquad (99)$$

and the energy equation for the top node becomes

$$\left[\overline{\rho_t c_t \Delta z} + L_{\ell i}\overline{\gamma_w \Delta z}\;\overline{F} + L_{vi}\overline{(\phi_{sd} - s\phi)\,\Delta z}\;\overline{f_{rh} C_{kT}}\right]\frac{\partial T}{\partial t} - \left(\overline{U_p - U_\ell^n}\right)\overline{H} + L_{\ell i}\left[\overline{U}_p\left(\overline{f_{\ell p}} - \overline{f_\ell}\right) - \overline{U}_\ell^n\left(1 - \overline{f_\ell}\right)\right] = \overline{I_{top}} - \overline{I_s\downarrow(1 - \alpha_{top})\left(e^{-\beta_\infty \Delta z}\, e^{-\beta_{nir}\, 0.002}\right)^n} + \overline{c_\ell\left(U_\ell T_\ell\right)^n} - \overline{\left(k_e \frac{\partial T}{\partial z}\right)^{n-\frac{1}{2}}} \qquad (100)$$

where

$$c_p \equiv f_{\ell p} c_\ell + (1 - f_{\ell p})\, c_i \;. \qquad (101)$$

DISCRETIZATION AND NUMERICAL IMPLEMENTATION

General structure of the model

In the preceding sections, governing equations were presented for the conservation of mass, momentum and energy within a snow–soil system. Each set contains n equations, one for each node or control volume. To solve the equations, they are first linearized and the differentials are approximated by discrete intervals. The solution procedure will now be outlined, where the reference numbers refer to the abbreviated flow-chart in Figure 6 and to the sections within the MAIN routine of the computer code.

At the inception of the computer run, necessary media and program parameters are read (Item 3), constant parameters are established (Item 4) and initial values are computed (Item 5). Subsequently the main time loop begins, which increments in time steps Δt automatically selected to obtain the desired accuracy of the solution. The first procedure within the time loop is to increment the meteorological data. Data are either provided from a meteorological file at a base sampling rate, which is usually once per hour (Item 6a) or, for intermediate time steps, is interpolated between past and current periods (Item 6b). Once the meteorological or driving parameters are established, the mass balance solution commences with the addition of snowfall or ponding rain to the top node (Item 7). This is followed by estimation of the compaction rate (Item 8), computation of elemental solar heating (Item 9), and estimation of the top boundary fluxes (Item 10). In the case of rain or melt, solutions are obtained for the fluid flow equations (Item 11), expressed in terms of the effective saturation s_e. Having established values for s_e, the water flux U_ℓ is computed from Darcy's equation, which in addition to the vapor flux U_v (Item 12a), is used to update the nodal mass (Item 13), thereby completing the mass balance section. Grain growth is estimated as a function of the vapor flux (Item 12b).

The energy balance section begins with updating of the thermal parameters (Item 14) and proceeds to the formulation and solution of the matrix of linear equations (Item 16). Both fluid flow and energy matrices assume a tridiagonal form and when linearized are solved using the tridiagonal-matrix algorithm (TDMA), described in Patankar (1980, p. 50–54) or Albert (1983). After solutions have been obtained to the energy equations, exact values for the linearized items are computed using the updated temperature values, and final adjustments are made to the liquid water parameters (Item 17). The equation balance is checked to see if the linearization error is acceptable (Item 18). If the convergence criteria are not met, the time step is reduced, values are reset, and the iteration is repeated. If the convergence criteria are met, the time step is retained or increased, current values are set to past values (Item 20), and processing continues. If an elemental thickness becomes less than 2 mm (through melt or evaporation), or if either of the top two nodes exceeds prescribed maxima, they are combined or subdivided (Item 21). Updated parameters are written to an output file at a rate chosen by the user (Item 22), which is usually that of the sampling rate of the input meteorological data. The time step or time loop is now complete, and the process is repeated for the next step, $t+\Delta t$.

Mass balance section

For computational efficiency, only the nodes with active water flow are included within the fluid flow matrix. The nodal system is subdivided into regions of contiguous flow as diagrammed in Figure 7, where the criteria for flow are that the effective saturation s_e exceed zero and that the element not be impermeable. Relative to the flow zone, the nodal index is denoted as $j' = j - ioffset$, where *ioffset* is the nodal offset between the bottom of the grid and the flow zone. For this version of the model, the condition of impermeable strata has been temporarily disallowed, pending further testing and verification of the saturated flow option. Discretization of the water flow equation proceeds directly from eq 46 and for the interior nodes takes the form

$$c7^j \left(s_e^{j,t} - s_e^{j,t-\Delta t}\right) = 0.5 \left\{Ak^{j+1}\left[s_e^3\right]^{j+1} - Ak^{j}\left[s_e^3\right]^{j}\right\}^{t} - 0.5 \left\{U_\ell^{j+1} - U_\ell^{j}\right\}^{t-\Delta t} + M^j \quad (102)$$

1. DECLARE ARRAYS and VARIABLE TYPES. Large common blocks are established in *ARRAYS*.

2. OPEN FILES. File names are read from *FILENAME*.

3. READ in general parameters and initial snowpack and soil element values for temperature, thickness, water content and grain size *(GETINPUT)*.

4. CALCULATE CONSTANT PARAMETERS for unfrozen water fraction, thermal conductivity, melt zone limits, bulk transfer functions over soil, water content limits, vapor diffusion and others *(CALCONSTANT)*.

5. INITIALIZE general liquid water variables *(DENSITY)*, combined specific heat and other miscellaneous parameters.

BEGIN TIME LOOP

6a. If this is the start of a basic time interval (default of 1 hour), then READ in or GENERATE METEOROLOGICAL DATA *(GETMET)* and screen it for out-of-bound data points. Optionally estimate solar radiation *(INSOL)* or downward long-wave radiation *(SKYRAD)* if measured values are not provided. Adjust measured or estimated radiation for incidence on sloped surface *(SLOPE)*.

6b. Automatically SUBDIVIDE basic time interval and INTERPOLATE meteorological data *(SUBTIME)*. Size of time step is determined in Section 18.

MASS BALANCE

7. ADD top elements, resulting from SNOWFALL or ponding RAIN *(NEWSNOW)*.

8. Determine COMPACTION rate of snow cover as a function of the initial settling rate and overburden *(COMPACT)*.

9. Estimate SOLAR HEATING within snow elements as a function of density and grain diameter *(SDSOL)*.

10. Estimate TOP BOUNDARY FLUXES, as functions of air temperature, wind speed, relative humidity and radiation *(QTURB)*.

11. For RAIN or MELT, compute the mass WATER FLOW exiting each element, using the gravity flow approximation of Colbeck and an upwind discretization scheme *(FILTRATE)*.

12a. Estimate mass transfer due to SUBLIMATION and DIFFUSION of WATER VAPOR within snow cover and for top node of bare soil *(DIFFUSION)*.

12b. Estimate SNOW GRAIN DIAMETER *(FGRAIN)*.

13. Using the snowfall rate and the estimates for water flow, vapor diffusion and compaction rate, UPDATE the SNOW DENSITY, MASS and elemental THICKNESS.

THERMAL BALANCE

14. Update THERMAL PARAMETERS, including effective thermal conductivity *(THRK)*; combined specific heat, slope of freezing curve, enthalpy adjustment factor and melt zone switches *(THPARAM)*.

15. For INITIAL TIME STEP, set PAST fluxes and variables.

16. SET UP and SOLVE linear THERMAL BALANCE equations, using tridiagonal matrix algorithm *(THERMAL, TRIDIAG)*. For elements in melt zone, compute temperature change from melt *(FTEMP)*. Recompute top fluxes using new temperature. Compute nodal heat fluxes (including solar heating) for use in next iteration *(FBB)*.

FINAL ADJUSTMENTS and PRINTOUT

17. Make final ADJUSTMENTS to LIQUID WATER variables *(DENSITY)*, determine melt state *(NMELT)* and make other adjustments.

18. CHECK if CONVERGENCE criteria are met *(CONVERGE)*. If not, reduce time step, reset variables and redo iteration. If met, increase time step and continue.

19. Optionally PRINT OUT surface FLUX and METEOROLOGICAL data for this basic time step *(FLUX)*.

20. SAVE PAST VALUES for mass, thermal and meteorological parameters *(OLD)*.

21. Divide or combine thick or thin snow elements *(SUBDIVIDE, COMBINENODES* and *COMBO)*.

22. PRINT OUT information for this basic time step *(WRITE)*. If measured temperatures are provided, compute RMS error.

END MAIN TIME LOOP

23. CLOSURE.

Figure 6. Abbreviated flow chart of SNTHERM.89. Major subroutines are indicated in upper-case italics.

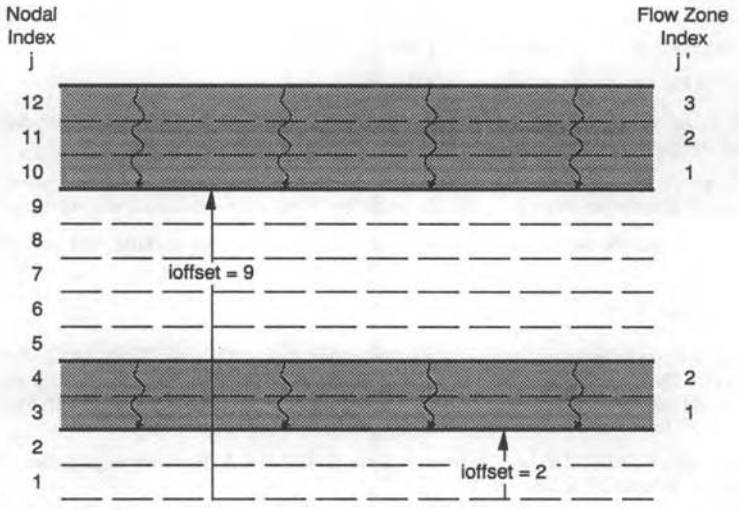

Figure 7. Diagram of flow zone system used in solution of fluid flow equations.

where $c7$, Ak and M are defined as

$$c7 \equiv \rho_\ell \frac{(1-s_r)\,\overline{\phi \Delta z}}{\Delta t} \approx \rho_\ell \frac{(1-s_r)\,(\phi \Delta z)^{t-\Delta t}}{\Delta t}$$

$$Ak \equiv \frac{\rho_\ell^2\, g\, K_{max}^{t}}{\mu_\ell} \approx \frac{\rho_\ell^2\, g\, K_{max}^{t-\Delta t}}{\mu_\ell} \tag{103}$$

and

$$M \equiv \overline{M_{\ell i}\, \Delta z} \left(1 - \frac{\rho_\ell}{\rho_i}\,\bar{s}\right) + \rho_\ell\, \overline{s\, \Delta z\, CR}$$

where the dynamic viscosity of water μ_ℓ is assumed to have a value of 1.787×10^{-3} N · s/m^2 at 0°C, and the procedure for estimating the phase change term M is described later. For the top node in the flow zone the discretized form is derived from eq 50 as

$$c7^j \left(s_e^{j,t} - s_e^{j,t-\Delta t}\right) = 0.5 \left\{ \frac{(f_{\ell p}\, \gamma_p\, fallrate)^{t-\Delta t} + (f_{\ell p}\, \gamma_p\, fallrate)^{t}}{3600} - Ak^j \left[s_e^3\right]^{j,t} + U_\ell^{j,t-\Delta t} \right\} + M^j$$

when $j = n$ and

$$c7^j \left(s_e^{j,t} - s_e^{j,t-\Delta t}\right) = 0.5 \left\{ - Ak^j \left[s_e^3\right]^{j} + U_\ell^{j,t-\Delta t} \right\} + M^j \tag{104}$$

when $j \neq n$, where the influx $U_\ell^{n+1} = (-f_{\ell p}\, \gamma_p\, fallrate)/3600$ when the flow zone is at the top of the snow pack and is otherwise zero.

Characteristic of gravity flow, the saturation profile generated by a water pulse propagating through snow approaches a step function at the wave front and has a comparatively gradual decline behind the receding edge of the pulse (Fig. 9). The term s_e^3 in eq 102 and 104 is therefore highly nonlinear for nodes at the wave front. Away from the front it can be linearized by the usual first-order Taylor's

expansion, as

$$(s_e^3)^t \approx b_s + m_s (s_e)^t$$

$$= -2 (s_e^3)^{t-\Delta t} + 3 (s_e^2)^{t-\Delta t} (s_e)^t \quad (105a)$$

if $j' \neq 1$ and $j' \neq n'$, where b_s and m_s are equation parameters estimated from the past effective saturation. At the front and for the top node it is estimated by obtaining a solution $s_{e,est}$ to the cubic equation:

$$0.5\, Ak^j \left(s^3_{e,est}\right)^j + c7^j s^j_{e,est} = c7^j s_e^{j,t-\Delta t} - U_\ell^{j+1,t-\Delta t} + 0.5\, U_\ell^{j,t-\Delta t} + M^j \quad (105b)$$

where it has been assumed that $U_\ell^{j+1,t} \approx U_\ell^{j+1,t-\Delta t}$, so that

$$(s_e^3)^t \approx 0 + m_s (s_e)^t$$

$$= 0 + s^2_{e,est} (s_e)^t \quad (105c)$$

if $j' = 1$ or $j' = n'$. For each flow zone a system of linear equations in s_e can be constructed, taking the standard tridiagonal-matrix form of

$$A_3^{j'} s_e^{j+1,t} + A_2^{j'} s_e^{j,t} = B^{j'} \quad (106)$$

where $A_1^{j'}$ is always 0 (because of the upwind scheme), and the matrix elements are defined as

$$A_3^{n'} = 0$$

$$A_2^{n'} = c7^j + 0.5\, Ak^j m_s^j$$

$$A_1^{n'} = 0$$

$$B^{n'} = -0.5\, U_\ell^{j+1,t} - 0.5 \left(U_\ell^{j+1} - U_\ell^j\right)^{t-\Delta t} + (c7\, s_e)^{j,t-\Delta t} + M^j \quad (107)$$

for the top node and

$$A_3^{j'} = -0.5\, Ak^{j+1} m_s^{j+1}$$

$$A_2^{j'} = c7^j + 0.5\, Ak^j m_s^j$$

$$A_1^{j'} = 0$$

$$B^{j'} = -0.5 \left(U_\ell^{j+1} - U_\ell^j\right)^{t-\Delta t} + (c7 s_e)^{j,t-\Delta t} + M^j + 0.5\, Ak^{j+1} b_s^{j+1} - 0.5\, Ak^j b_s^j \quad (108)$$

for the interior nodes. The numerical solution becomes unstable if an initially dry node is totally saturated in one time step. To assure accuracy and stability of the solution, the minimum time step limit Δt_{min} for the adaptive time step range should meet the empirically derived criterion

$$\Delta t_{\min} < \frac{0.5\,\Delta z_{\min}}{-U_\ell^{n+1}+M} \tag{109}$$

where $\Delta z_{\min}$ (m) is the thickness of the thinnest node. Further discussion of the minimum time step versus solution accuracy is presented later.

The effective saturation reaches a steady-state value $\tilde{s}_e$ when the nodal outflux equals the influx, which for a water source of constant magnitude is computed as

$$\tilde{s}_e = \sqrt[3]{\left(\frac{-U_\ell^{n+1}+M}{\frac{\rho_\ell^2\, g\, K_{\max}}{\mu_\ell}}\right)} = \sqrt[3]{\left(\frac{\rho_\ell \frac{fallrate}{3600}+M}{Ak}\right)} \tag{110}$$

Employing conservation of mass, the wave front in a snow cover with an antecedent water content at or below the residual saturation level then propagates at an approximate speed of*

$$v \approx \frac{\textit{Surface influx rate}}{\textit{Residual saturation deficit} + \textit{Thermal deficit} + \textit{Drainable water}}$$

$$= \frac{-U_\ell^{n+1}+M}{\rho_\ell\,(s_r - s_0)\,\phi + \frac{\gamma_i c_i (T_D)}{L_{\ell i}} + \rho_\ell \tilde{s}_e (1-s_r)\,\phi} \tag{111}$$

where the thermal deficit is the amount of influx frozen in warming the snow cover to 0°C, the drainable water is the steady-state level of liquid water in excess of the residual or immobile water content, and s_0 is the antecedent saturation. Following cessation of the surface water flux, the snow cover drains to its residual saturation level.

Colbeck (1976) computed runoff at the bottom of a 1-m-deep snow pack for hypothetical cases of fresh, ripe and refrozen snow. The water source in each case was a heavy rainfall of 0.01 mm/s, or 1.42 in./hour. For fresh and refrozen snow the temperature was initialized at –5°C, so that a heat deficit as well as the residual saturation deficit had to be satisfied prior to advancement of the water front. A small grain size of 0.2 mm was used for fresh snow, compared with 2.0 mm for the older snow types, reducing the saturation permeability and substantially slowing the flow of water. Model predictions of runoff for the three cases as compared with Colbeck's results are shown in Figure 8, and the assumed physical parameters and model results are summarized in Table 1. Since porosity changes and grain growth are not considered in Colbeck's solution, these mechanisms have been disabled in the computation of the flow coefficient A_k for the model simulations.† Agreement between the two procedures is generally good, except that lag times predicted by the model for the cold snow cases are about 10% longer. Colbeck** indicated that he used a graphic procedure and that the numerical solution should be more accurate. The slight dispersion about the wave front in the model solution is an artifact of the numerical method, and it reduces to the expected shock front solution as the nodal thickness is reduced. In actuality the numerical simulation is more representative of hydrographs from real snow covers, as inhomogeneities in snow characteristics lead to a spread in the flow rates.

---

* For a complete discussion of the rate of propagation of a wave front in melting snow, see Colbeck (1974a).

† Computation of the steady-state mass gains in Table 1 take porosity changes due to freezing into account, since it was too difficult to exclude them from the model.

** Personal communication, 1991.

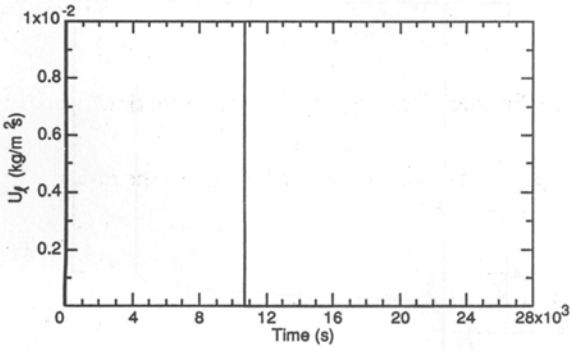

a. Incident surface flux of 0.01kg/m^2·s for a duration of 10,800 s.

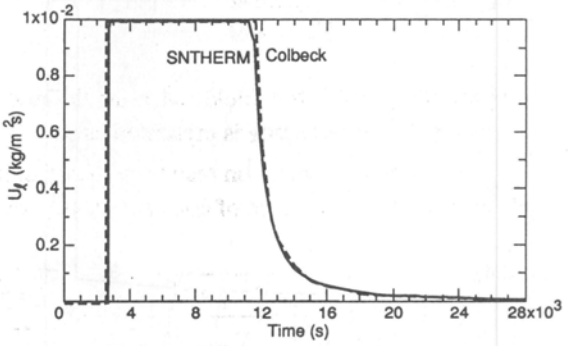

b. SNTHERM model predictions and computations of Colbeck (1976) for ripe snow.

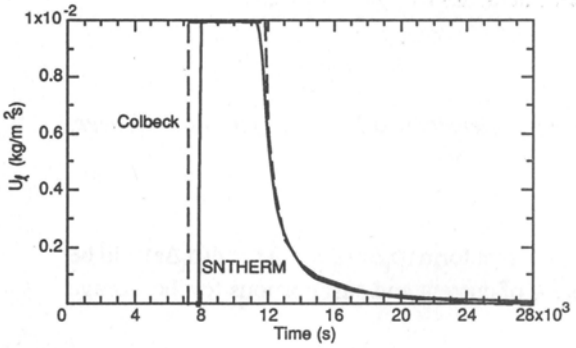

c. SNTHERM model predictions and computations of Colbeck (1976) for refrozen snow.

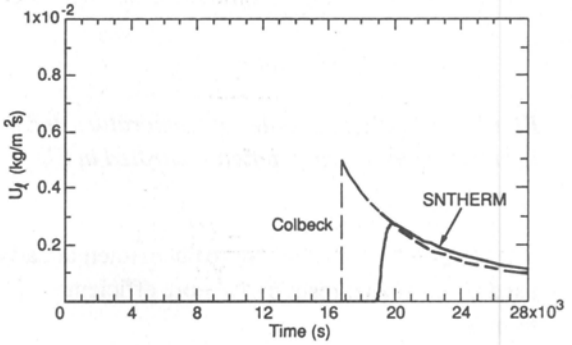

d. SNTHERM model predictions and computations of Colbeck (1976) for fresh snow.

Figure 8. Mass water flux at the bottom of a 1-m-deep snow cover.

Table 1. Assumed snow parameters and model predictions of water infiltration in fresh, ripe and refrozen snow covers. The snow cover is 1 m deep, and the incident flux has a constant magnitude of 0.01 kg/m^{-2}·s and duration of 10,800 s.

	ρ_s (kg/m^3)	d (mm)	T_0 (°C)	ϕ	Lag (s)	Steady-state effective saturation	Ak (kg/m^2·s)	Steady-state mass gain (kg/m^3)	Immobile liquid influx (kg/m^3)	Frozen influx (kg/m^3)	Drainable influx (kg/m^3)
Ripe	300	2.0	0	0.73	2,254	0.035	242	24	0	0	24
Refrozen	300	2.0	–5	0.67	7,978	0.039	163	80	46	10	24
Fresh	300	0.2	–5	0.67	18,615	0.183	1.63	169	46	10	113

In addition to illustrating the water flow algorithm, the two cases of rain on cold snow demonstrate the coupled heat and mass flow capability of the model. Temperature and bulk liquid density profiles predicted by the model for the fresh snow case are shown in Figure 9. The liquid density reaches a steady-state level of 159 kg/m^3 and then gradually drains towards the residual level of 46 kg/m^3.

Energy balance section

Once the fluid flows and adjusted mass balances have been computed, the energy balance equation (eq 74 and 100) can be solved for the nodal temperature or phase change. First the heat storage terms on the left side of eq 74 are discretized, which correspond to the partial derivative $\partial(\rho_t \Delta z h_t)/\partial t$ in eq 59. Usually the discretized form of the product $(\rho_t \Delta z)h_t$ would be $0.5[(\rho_t \Delta z)^t + (\rho_t \Delta z)^{t-\Delta t}]\Delta h_t + 0.5(h_t^t$

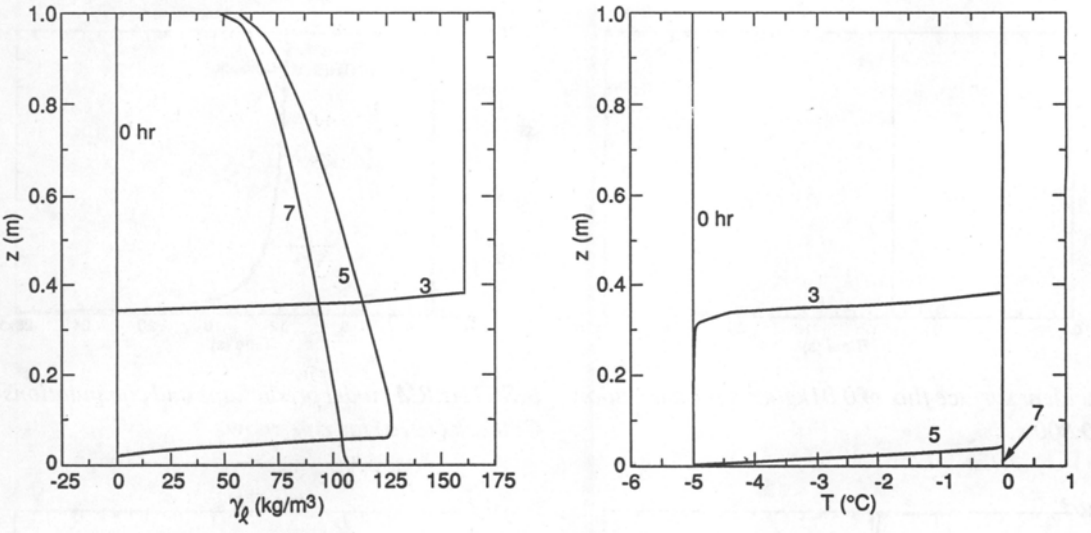

a. Bulk liquid density. *b. Temperature.*

Figure 9. Predicted profiles of temperature and bulk liquid density in a 1-m-deep fresh snow cover, in response to the input pulse illustrated in Figure 8a.

$+h_t^{t-\Delta t})\Delta(\rho_t \Delta z)$. An alternative but mathematically equivalent form $(\rho_t \Delta z)^t \Delta h_t + h_t^{t-\Delta t}\Delta(\rho_t \Delta z)$ will be used here, since it results in a more efficient partitioning of current and past portions for the storage term, as

$$\frac{\partial(\rho_t \Delta z) h_t}{\partial t} - \left(\overline{U_\ell^{j+1} - U_\ell^j}\right)(c_\ell\, 273.15 - L_{\ell i}) =$$

$$\left[\overline{\rho_t c_t \Delta z} + L_{\ell i}\overline{\gamma_w \Delta z}\;\overline{F} + L_{vi}\overline{(\phi_{sd} - s\phi)\Delta z}\;\overline{f_{rh} C_{kT}}\right]\frac{\partial T}{\partial t} - \left(\overline{U_\ell^{j+1} - U_\ell^j}\right)\left[\overline{H} - L_{\ell i}\left(1 - \overline{f_\ell}\right)\right]$$

$$= \left\{\Delta z\left[\rho_t c_t + L_{\ell i}\gamma_w \overline{F} + L_{vk}\overline{(\phi_{sw} + s\phi)}\,\overline{f_{rh} C_{kT}}\right]\right\}^{j,t}\frac{T^{j,t} - T^{j,t-\Delta t}}{\Delta t}$$

$$- \left(\overline{U_\ell^{j+1} - U_\ell^j}\right)\left[H - L_{\ell i}\left(1 - f_\ell\right)\right]^{j,\,t-\Delta t} \quad . \tag{112}$$

Furthermore it can be shown that

$$\left(\Delta z\,\gamma_w \overline{F}\right)^{j,t}\frac{T^{j,t} - T^{j,\,t-\Delta t}}{\Delta t} - \left(\overline{U_\ell^{j+1} - U_\ell^j}\right) f_\ell^{\,j,\,t-\Delta t}$$

$$= \left\{\Delta z\,\gamma_w \overline{\overline{F}}\,[T, \gamma_w(t)]\right\}^{j,\,t}\frac{T^{j,\,t} - T^{j,\,t-\Delta t}}{\Delta t} - \left(\overline{U_\ell^{j+1} - U_\ell^j}\right)\hat{f}_\ell^{\,j,\,t-\Delta t} \tag{113}$$

where $\overline{\overline{F}}\,[T, \gamma_w(t)]$ is the temporal average of F (eq 68) in temperature evaluated for the *current* water content γ_w^t, and $\hat{f}_\ell$ is the portion of the freezing curve (eq 67) that is independent of water content, given as

$$\hat{f}_\ell \equiv \frac{1}{1 + (a1\, T_d)^2}. \tag{114}$$

Applying a central-difference scheme for the conduction–diffusion term and an upwind scheme for the convection term, we can write the discretized version of the energy equation (eq 74) as

$$\left\{\Delta z\left[\rho_t c_t + L_{\ell i}\gamma_w \overline{\overline{F}} + L_{vi}\,\overline{(\phi_{sw} + s\phi)}\,\overline{f_{rh}\, C_{kT}}\right]\right\}^{j,t} \frac{T^{j,t} - T^{j,t-\Delta t}}{\Delta t}$$

$$- \overline{U}^{j}_{\ell,net}\left[H - L_{\ell i}(1 - \hat{f}_\ell)\right]^{j,t-\Delta t} = -c_\ell\left[U_\ell^{j+1}\,\frac{T^{j+1}}{2} - U_\ell^{j}\,\frac{T^{j}}{2}\right]^{t}$$

$$+\left[\frac{\hat{k}_e^{\,j+\frac{1}{2}}\left(T^{j+1} - T^{j}\right) - \hat{k}_e^{\,j-\frac{1}{2}}\left(T^{j} - T^{j-1}\right)}{2}\right]^{t} + \left[\frac{I_s^{j+\frac{1}{2}}}{2}\left(1 - e^{-\beta_\infty \Delta z}\right)\right]^{t} + \frac{Q_{net}^{j,t-\Delta t}}{2} \tag{115}$$

where $\hat{k}_e^{\,j+\frac{1}{2}}$ and $\hat{k}_e^{\,j-\frac{1}{2}}$ are derived from the steady-state conductivities:

$$\hat{k}_e^{\,j+\frac{1}{2}} \equiv \frac{2k_e^j k_e^{j+1}}{k_e^j \Delta z^{j+1} + k_e^{j+1}\Delta z^j}$$

and

$$\hat{k}_e^{\,j-\frac{1}{2}} \equiv \frac{2k_e^j k_e^{j-1}}{k_e^j \Delta z^{j-1} + k_e^{j-1}\Delta z^j}. \tag{116}$$

The average net liquid water flux is

$$\overline{U}^{j}_{\ell,net} \equiv \frac{\left(U_\ell^{j+1} - U_\ell^{j}\right)^{t} + \left(U_\ell^{j+1} - U_\ell^{j}\right)^{t-\Delta t}}{2} \tag{117}$$

and the past net heat fluxes Q_{net} are

$$Q_{net}^{n,t-\Delta t} \equiv I_{top}^{t-\Delta t} + c_\ell\,(U_\ell T)^{n,t-\Delta t} - \left[\hat{k}_e^{\,n-\frac{1}{2}}\left(T^n - T^{n-1}\right)\right]^{t-\Delta t}$$

$$- \left[I_s{\downarrow}\left(1 - \alpha_{top}\right)\left(e^{-\beta_\infty \Delta z}\, e^{-\beta_{nir}\, 0.002}\right)\right]^{n,t-\Delta t} \tag{118a}$$

for the top node and

$$Q_{net}^{j,t-\Delta t} \equiv -c_\ell\left[(U_\ell T)^{\,j+1} - (U_\ell\ T)^{j}\right]^{t-\Delta t}$$

$$+\left[\hat{k}_e^{\,j+\frac{1}{2}}\left(T^{j+1} - T^{j}\right) - \hat{k}_e^{\,j-\frac{1}{2}}\left(T^{j} - T^{j-1}\right)\right]^{t-\Delta t} + \left[I_s^{j+\frac{1}{2}}\left(1 - e^{-\beta_\infty \Delta z}\right)\right]^{t-\Delta t} \tag{118b}$$

for the interior nodes. Equation 115 is the final discretized form of the heat balance equation for the interior nodes.

Values for the phase change term M in the fluid flow equation are estimated from eq 62 by assuming that the nodal temperatures, and the convective and conductive fluxes, are constant over the time step. Using eq 24, 103 and 117

$$M \equiv \overline{M_{\ell i}\,\Delta z}\left(1-\frac{\rho_\ell}{\rho_i}\bar{s}\right)+\rho_\ell\,\overline{s\,\Delta z\,CR}$$

$$=\left[\frac{(\gamma_\ell\Delta z)^t-(\gamma_\ell\Delta z)^{t-\Delta t}}{\Delta t}+\bar{U}^j_{\ell,\mathrm{net}}\right]\left(1-\frac{\rho_\ell}{\rho_i}\bar{s}\right)+\rho_\ell\,\overline{s\,\Delta z\,CR}\ .$$

Then using eq 62, 77 and 118

$$M \approx \left\{\frac{Q^{n,t}_{\mathrm{solar}}+I'_{\mathrm{top,k}}+I'_{\mathrm{top,v}}\,T^{n,t-\Delta t}+c_\ell\left(U_\ell T\right)^n-\left[\hat{k}_e^{\,n-\frac{1}{2}}\left(T^n-T^{n-1}\right)\right]^{t-\Delta t}}{2}+\frac{Q^{n,t-\Delta t}_{\mathrm{net}}}{2}\right.$$

$$\left.+\left(\frac{U^{n+1,t}+U^{n+1,t-\Delta t}}{2}-U^{n,t-\Delta t}\right)H^{n,t-\Delta t}\right\}$$

$$\times\left(1-\frac{\rho_\ell}{\rho_i}s^{n,t-\Delta t}\right)/L_{\ell i}+\rho_\ell\left(s\Delta z\,CR\right)^{n,t-\Delta t} \qquad (119a)$$

for the top node and

$$M \approx \left\{Q^{j,t-\Delta t}_{\mathrm{net}}+\frac{\left(Q^{j,t}_{\mathrm{solar}}-Q^{j,t-\Delta t}_{\mathrm{solar}}\right)}{2}+\left[\left(U^{j+1}-U^j\right)H^j\right]^{t-\Delta t}\right\}$$

$$\left(1-\frac{\rho_\ell}{\rho_i}s^{j,t-\Delta t}\right)/L_{\ell i}+\rho_\ell\left(s\Delta z\,CR\right)^{j,t-\Delta t} \qquad (119b)$$

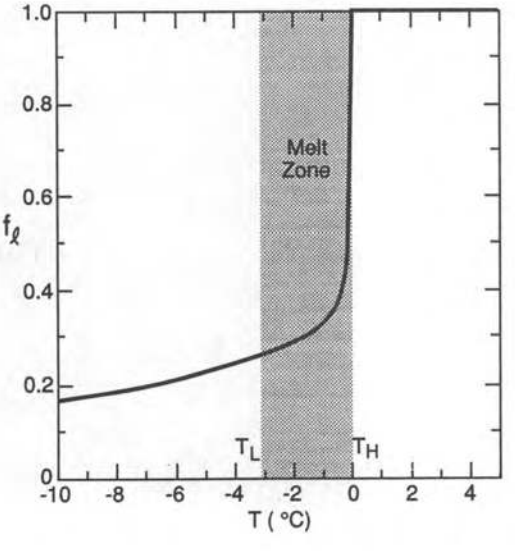

Figure 10. Conceptualization of the melt zone ($T_L<T<T_H$), where P_{melt} rather than T is used as the independent variable in the heat balance equation.

for the interior node. The air interface fluxes I'_{top} are defined in eq 124 and 125. Since the time steps are very small when melt is occurring, the subsequent version of the model will estimate melt from its past value, thereby avoiding these complicated expressions.

Solving eq 115 requires that terms first be linearized, which in most cases is accomplished by using past values to estimate current values. Near 0°C the slope of the freezing curve F changes rapidly with temperature, so that maintaining acceptable linearization error for elements undergoing melt leads to very small time steps. To improve computational efficiency, melt is used instead of temperature as the independent variable in this region of the freezing curve. The approximation uncertainty is thereby shifted from the latent to the sensible heat change, which is of much lower magnitude. The region where this variable transformation applies is termed the "melt zone," as shown in Figure 10 and is arbitrarily bounded by the limits T_L and T_H on the freezing curve where sensible and latent heat changes approach the same magnitude, given as

$$T_L = 273.15 - \left[\frac{2\,L_{\ell i}}{a1^2\left(c_i + \frac{\gamma_d c_d}{\gamma_{w,mid}}\right)}\right]^{\frac{1}{3}} \tag{120}$$

and

$$T_H = 273.15 - \left(\frac{c_\ell + \frac{\gamma_d c_d}{\gamma_{w,mid}}}{2L_{\ell i}a1^2}\right)$$

where $\gamma_{w,mid}$ is the midpoint bulk water density in soil between the residual and saturation limits. A melt function P_{melt} is introduced, defined as the change in γ_ℓ with temperature over the time step in which the bulk water density is held constant at its current value γ_w^t, or

$$P_{melt} \equiv \gamma_w^t\left[f_\ell\left(T^t, \gamma_w^t\right) - f_\ell\left(T^{t-\Delta t}, \gamma_w^t\right)\right]$$

$$= \gamma_w^t f_\ell^t - \frac{\gamma_w^t - 0.75\,\gamma_d J_p}{1 + \left[(a1\,T_d)^2\right]^{t-\Delta t}} - \frac{0.75\,\gamma_d J_p}{1 + \left[(a2\,T_d)^{\frac{4}{3}}\right]^{t-\Delta t}} \approx \gamma_w^t\,\overline{\overline{F}}\,\Delta T \tag{121}$$

where $\overline{\overline{F}}$ was defined in eq 113. Temperature is then expressed in terms of P_{melt} as

$$T^{j,t} = g_v^j\,P_{melt}^{j,t} + g_k^j \tag{122a}$$

where within the melt zone when $T_L \le T^{j,t-\Delta t} \le T_H$

$$g_v^j \equiv \frac{1}{\gamma_w^t\,\overline{\overline{F}}^j}$$

and

$$g_k^j \equiv T^{j,t-\Delta t} \tag{122b}$$

The variables g_v and g_k function as switches within the linear equation system, automatically transforming P_{melt} to T when an element is within the melt region. Outside of the melt zone when $T^{j,t-\Delta t} < T_L$ or $T^{j,t-\Delta t} > T_H$ these functions are defined as

$$g_{\mathrm{v}}^{j} \equiv 1$$

and

$$g_{\mathrm{k}}^{j} \equiv 0 \,. \tag{123}$$

The combined heat flux at the air interface $I_{\mathrm{top}}^{'}$ is linearized in terms of temperature, where $I_{\mathrm{top,\,k}}^{'}$ is the constant term and $I_{\mathrm{top,\,v}}^{'}$ is the coefficient on T, as*

$$I_{\mathrm{top}}^{'} \equiv I_{\mathrm{top,\,k}}^{'} + I_{\mathrm{top,\,v}}^{'} T^{n} \tag{124}$$

where†

$$I_{\mathrm{top,\,k}}^{'} \equiv 0.5 \left\{ \varepsilon I_{\mathrm{ir}}\downarrow + \left(E_{\mathrm{H0}} + E_{\mathrm{H}}w\right) T_{\mathrm{air}} + \left(E_{\mathrm{E0}} + E_{\mathrm{E}}w\right) \left(P_{\mathrm{v,\,air}} + 21.452\, f_{\mathrm{rh}}\, P_{\mathrm{vk,sat}}^{n,\,t-\Delta t}\right) \right.$$

$$\left. + 3\sigma\varepsilon \left(T^{4}\right)^{n,\,t-\Delta t} - c_{\mathrm{p}}\, T_{\mathrm{p}} U_{\mathrm{p}} \right\}$$

and

$$I_{\mathrm{top,\,v}}^{'} \equiv -0.5 \left\{ \left(E_{\mathrm{H0}} + E_{\mathrm{H}}w\right) + 22.452\, \frac{f_{\mathrm{rh}}\, P_{\mathrm{vk,\,sat}}^{n,\,t-\Delta t} \left(E_{\mathrm{E0}} + E_{\mathrm{E}}w\right)}{T^{\,n,\,t-\Delta t}} + 4\sigma\varepsilon \left(T^{3}\right)^{n,\,t-\Delta t} \right\}. \tag{125}$$

In these relationships all quantities are evaluated for the current time unless otherwise indicated, and the following approximations have been made:

$$\left(T^{4}\right)^{t} \approx \left(T^{4}\right)^{t-\Delta t} + 4\left(T^{3}\right)^{t-\Delta t} \left(T^{t} - T^{\,t-\Delta t}\right) = \left(T^{3}\right)^{t-\Delta t} \left(4T^{t} - 3T^{\,t-\Delta t}\right) \tag{126}$$

$$P_{\mathrm{vk,\,sat}}^{t} \approx P_{\mathrm{vk,\,sat}}^{\,t-\Delta t} \left[22.452\, \frac{T^{t}}{T^{\,t-\Delta t}} - 21.452 \right]$$

$$E_{\mathrm{H}}^{t} \approx E_{\mathrm{H}}^{\,t-\Delta t}$$

$$E_{\mathrm{E}}^{t} \approx E_{\mathrm{E}}^{\,t-\Delta t} \,.$$

The equation system can now be written in standard tridiagonal form as

$$A_3^{j} X^{\,j+1,\,t} + A_2^{j} X^{\,j,\,t} + A_1^{j} X^{\,j-1,\,t} = B^{j} \tag{127}$$

where $X = T$ when a node is outside the melt zone and $X = P_{\mathrm{melt}}$ when it is within the melt zone. The matrix elements of A and B are defined as

$$A_3^{n} = 0.0$$

---

* The term $I_{\mathrm{top}}^{'}$ used here is inconsistent with I_{top} defined in eq 75, in that it does not contain the solar flux.
† The case of falling wet snow is addressed in the equations but is not included in the SNTHERM.89 code.

$$A_2^n = Q_s^n - c_\ell \frac{U^{n,t}}{2} + \frac{\hat{k}_e^{n-\frac{1}{2},t}}{2} - I'_{\text{top, v}} \quad \text{when} \quad T_L^{n,t-\Delta t} < T_L \text{ or } T^{n,t-\Delta t} > T_H$$

$$A_2^n = \left(Q_s^n - c_\ell \frac{U^{n,t}}{2} + \frac{\hat{k}_e^{n-\frac{1}{2},t}}{2} - I'_{\text{top, v}}\right) g_v^n + L_{\ell i} \frac{\Delta z^{n,t}}{\Delta t} \quad \text{when} \quad T_L^{n,t-\Delta t} \le T^{n,t-\Delta t} \le T_H$$

$$A_1^n = -\frac{\hat{k}_e^{n-\frac{1}{2},t}}{2} g_v^{n-1}$$

$$B^n = Q_s^n T^{n,t-\Delta t} + \left\{\overline{U}_{\ell,\text{net}} H - L_{\ell i}\left[\overline{U}_p\left(\bar{f}_{\ell p} - \hat{f}_\ell\right) - \overline{U}_\ell\left(1 - \hat{f}_\ell\right)\right]\right\}^{n,t-\Delta t}$$

$$+\left[I_s \downarrow \left(1 - \alpha_{\text{top}}\right) \frac{\left(1 - e^{-\beta_\infty \Delta z}\, e^{-\beta_{\text{nir}}\, 0.002}\right)}{2}\right]^{n,t} + \frac{Q_{\text{net}}^{n,t-\Delta t}}{2}$$

$$-\left\{-\frac{\hat{k}_e^{n-\frac{1}{2},t}}{2} g_k^{n-1} + \left(Q_s^n - c_\ell \frac{U^{n,t}}{2} + \frac{\hat{k}_e^{n-\frac{1}{2},t}}{2} - I'_{\text{top, v}}\right) g_k^n\right\} + I'_{\text{top, k}} \tag{128}$$

for the top nodes,

$$A_3^j = \left(\frac{c_\ell U^{j+1,t}}{2} - \frac{\hat{k}_e^{j+\frac{1}{2},t}}{2}\right) g_v^{j+1}$$

$$A_2^j = Q_s^j - c_\ell \frac{U^{j,t}}{2} + \frac{\hat{k}_e^{j+\frac{1}{2},t} + \hat{k}_e^{j-\frac{1}{2},t}}{2} \quad \text{when} \quad T_L^{j,t-\Delta t} < T_L \text{ or } T_L^{j,t-\Delta t} > T_H$$

$$A_2^j = \left(Q_s^j - c_\ell \frac{U^{j,t}}{2} + \frac{\hat{k}_e^{j+\frac{1}{2},t} + \hat{k}_e^{j-\frac{1}{2},t}}{2}\right) g_v^j + L_{\ell i} \frac{\Delta z^{j,t}}{\Delta t} \quad \text{when} \quad T_L \le T^{j,t-\Delta t} \le T_H$$

$$A_1^j = -\frac{\hat{k}_e^{j-\frac{1}{2},t}}{2} g_v^{j-1}$$

$$B^j = Q_s^j T^{j,t-\Delta t} + \overline{U}_{\ell,\text{net}}^j \left[H - L_{\ell i}\left(1 - \hat{f}_\ell\right)\right]^{j,t-\Delta t} + \left[I_s^{j+\frac{1}{2}} \frac{\left(1 - e^{-\beta_\infty \Delta z}\right)^j}{2}\right]^t + \frac{Q_{\text{net}}^{j,t-\Delta t}}{2}$$

$$-\left[-\frac{\hat{k}_e^{j-\frac{1}{2},t}}{2} g_k^{j-1} + \left(Q_s^j - c_\ell \frac{U^{j,t}}{2} + \frac{\hat{k}_e^{j+\frac{1}{2},t} + \hat{k}_e^{j-\frac{1}{2},t}}{2}\right) g_k^j + \left(\frac{c_\ell U^{j+1,t}}{2} - \frac{\hat{k}_e^{j+\frac{1}{2},t}}{2}\right) g_k^{j+1}\right] \tag{129}$$

for the interior nodes and

$$A_3^1 = 0.0 \tag{130}$$

$$A_2^1 = B^1$$

$$A_1^1 = 0.0$$

$$B^1 = T^1_{\text{constant}}$$

for the bottom node. The following definitions and linearizations are used:

$$Q_s^j \equiv \left\{\left[\rho_t c_t + L_{\ell i}\gamma_w \overline{\overline{F}} + L_{vi}\left(\overline{\phi_{sd} - s\phi}\right)\overline{f_{rh} C_{kT}}\right]\frac{\Delta z}{\Delta t}\right\}^{j,t}$$

$$\text{when } T^{j,t-\Delta t} < T_L \text{ or } T^{j,t-\Delta t} > T_H$$

$$Q_s^j \equiv \left\{\left[\rho_t c_t + L_{vi}\left(\overline{\phi_{sd} - s\phi}\right)\overline{f_{rh} C_{kT}}\right]\frac{\Delta z}{\Delta t}\right\}^{j,t}$$

$$\text{when } T_L \le T^{j,t-\Delta t} \le T_H \tag{131}$$

$$\overline{c_t} \approx c_t^{t-\Delta t}$$

$$\overline{\overline{F}}_{kT} \approx \hat{F}_{kT}^{t-\Delta t}$$

$$\overline{C}_{kT} \approx C_{kT}^{t-\Delta t}$$

$$\phi^t,\ \phi_{sd}^t \approx \phi^{t-\Delta t},\ \phi_{sd}^{t-\Delta t}.$$

When new elements are created to accommodate the accumulation of snowfall or ponding water, the numerical solution is unstable until a minimum elemental mass is reached. In this case the thermal balance is circumvented, and the nodal temperature is set to that of the precipitation.

Final adjustments and adaptive time step procedure

For nodes within the melt zone, the function P_{melt} (eq 121), rather than temperature, is returned by the solution to the heat balance equation. For these nodes the current bulk liquid-water density is computed from P_{melt} as

$$\gamma_\ell^t = P_{melt} + \frac{\left(\gamma_\ell^t \Delta z\right)^{t-\Delta t} - \overline{U}_{\ell,net}\hat{f}_\ell^{t-\Delta t}\Delta t}{\Delta z^t} \tag{132}$$

and eq 67 is then solved for T as

$$T = 273.15 - \frac{1}{a1}\sqrt{\frac{\gamma_w^t}{\gamma_\ell^t} - 1} \tag{133a}$$

for snow and

$$\left(T_D^{\frac{2}{3}}\right)^5 + p\left(T_D^{\frac{2}{3}}\right)^3 + q\left(T_D^{\frac{2}{3}}\right)^2 = \hat{s} \tag{133b}$$

for soil, where the coefficients in the fifth-order polynomial for soil are given as

$$p = \frac{1 - 0.75\,\frac{\gamma_d}{\gamma_\ell^t}\,J_p}{a2^{\frac{4}{3}}} \tag{134}$$

$$q = \frac{1 - \frac{\gamma_w^t}{\gamma_\ell^t} - 0.75\,\frac{\gamma_d}{\gamma_\ell^t}\,J_p}{a1^2}$$

$$\hat{s} = \frac{1 - \frac{\gamma_w^t}{\gamma_\ell^t}}{a1^2 a2^{\frac{4}{3}}} .$$

Equation 133b is solved iteratively using the Newton–Raphson bisection technique. Since eq 122a will not provide valid solutions in the eventuality that a phase boundary is extremely overshot, a check is first made to see if P_{melt} has exceeded a boundary by more than 5%. This should not normally occur, since the time step is automatically shortened as the boundary is approached, but if the situation should arise, the step is shortened and the iteration is repeated.

Given the new set of temperatures, the top flux (eq 124) is recomputed, and new values for the liquid water density, saturation, unfrozen mass fraction and porosity are established. Substituting into the original form of the heat equation (eq 62), we can compute the linearization error in the energy balance and express it as an effective temperature error T_{error}, where

$$T_{error} = \frac{\Delta t \; Heat\ balance\ error}{\left\{\Delta z \left[\rho_t c_t + L_{vi}\left(\overline{\phi_{sd} - s\phi}\right)\overline{f_{rh}\, C_{kT}}\right]\right\}^t} . \tag{135}$$

A minimum allowable error is input to the model, typically 0.05°C. If the error tolerance is exceeded, the time step is shortened, nodal parameters are reset and the iteration is repeated. Conversely, if the error is below the tolerance level, the time step is increased. For a given linearization error, note that decreasing the nodal thickness leads to smaller time steps. In the case where the thermal balance has been circumvented due to minimal mass or when a node is being deleted, the convergence check is bypassed. A convergence check is also included so that changes in water saturation within a time step remain below a specified level.

Combination and subdivision of elements

Combination

If a snow element has totally melted or if its thickness is less than the prescribed minimum of 2 mm (*except* if it is a new element accumulating precipitation), the element is combined with a neighboring element. The top or bottom neighbor is selected as the recipient according to the following criteria:

- If the surface element is being removed, combine it with the bottom neighbor;
- If the bottom neighbor is not snow, combine it with the top neighbor;
- If the element is entirely melted, combine it with the bottom neighbor; and
- If none of the above cases apply, combine it with the thinnest neighbor.

The two elements are combined by adding the thicknesses and masses, and computing the combined bulk density as

$$\gamma_w^c = \frac{\gamma_w^1 \Delta z^1 + \gamma_w^2 \Delta z^2}{\Delta z^1 + \Delta z^2} = \frac{mass^1 + mass^2}{\Delta z^c} = \frac{mass^c}{\Delta z^c} \tag{136}$$

where the superscripts 1, 2 and c denote the separate and combined elements, respectively. Mass weights are used to compute a combined grain size of

$$d^c = \frac{d^1 mass^1 + d^2 mass^2}{mass^c} \tag{137}$$

and a combined temperature for dry snow of

$$T^c = \frac{T^1 mass^1 + T^2 mass^2}{mass^c} . \tag{138}$$

In the case of wet snow the sum of the enthalpies of the separate elements is equated to that of the combined element, as

$$- c_i \left(mass^1 T_D^1 + mass^2 T_D^2 \right) + L_{\ell i} \left(\gamma_\ell^1 \Delta z^1 + \gamma_\ell^2 \Delta z^2 \right)$$

$$= - c_i \, mass^c \, T_D^c + L_{\ell i} \, \gamma_\ell^c \, \Delta z^c . \tag{139}$$

Using eq 67 to express γ_ℓ^c, eq 139 is written as a third-order polynomial, which is solved iteratively for T_D^c using the Newton–Raphson technique, in which the solution is bounded by T_D^1 and T_D^2. The past values for the net fluxes Q_{net} and the elemental solar absorption Q_{solar} are combined additively as

$$Q_{net}^1 + Q_{net}^2 = Q_{net}^c$$

and

$$Q_{solar}^1 + Q_{solar}^2 = Q_{solar}^c . \tag{140}$$

Nodes superior to the combined node are shifted down by one index number, and parameters for the former top node are set to 0. Re-definition and re-indexing of nodal values is facilitated by declaring the nodal vectors equivalent to large two-dimensional arrays defined within the subroutine *ARRAYS*.

Subdivision

The two uppermost nodes are automatically subdivided if they exceed the prescribed minimum values of $1^2/3$ and $3^1/3$ cm. If the $(n-1)^{th}$ node is being subdivided, the top node is first moved up by one index number. Subsequently a new node is created that has the same values as the original node. The procedure is completed by readjusting mass-related variables so that a third of the mass is assigned to the upper node and two thirds to the lower node of the pair.

MODEL VERIFICATION

The ability of SNTHERM.89 to predict surface temperatures has been verified on field data for several years from sites in Grayling, Michigan, and Hanover, New Hampshire. The instrumentation consisted of thermocouple profiles within the snow and soil, an adjustable surface probe, a meteoro-

logical tower instrumented at two or three levels for measuring air temperature, wind speed and relative humidity, and pairs of Eppley pyranometers and pyrgeometers for measuring upwelling and downwelling radiation. A detailed description of the Hanover test site is presented in Jordan et al. (1989). Comparison of measured to predicted surface temperatures for snow showed agreement to within ±1.0–1.5°C for diurnal temperature cycles of amplitude up to 20°C, with most of the discrepancy occurring over midday when the thermocouples overheated due to solar loading. Figure 11

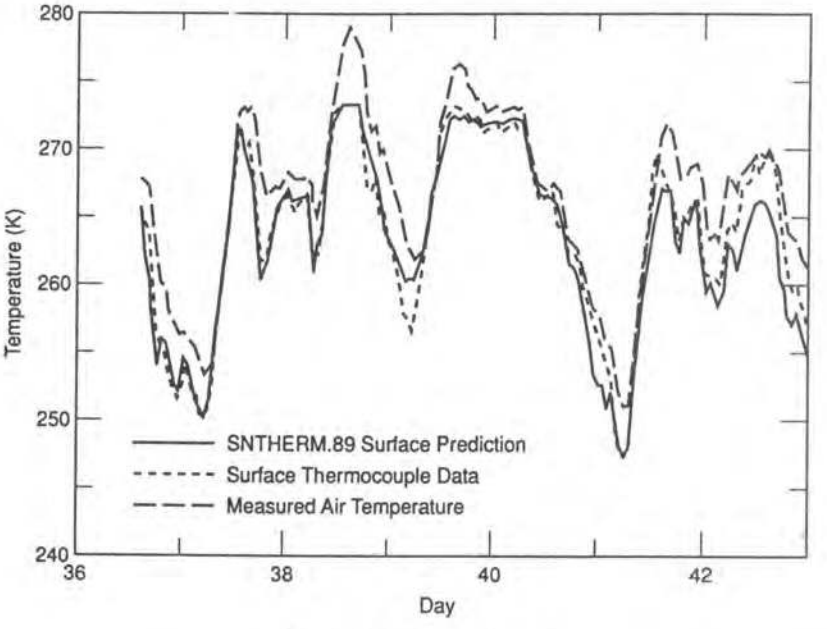

a. 5–11 February 1987.

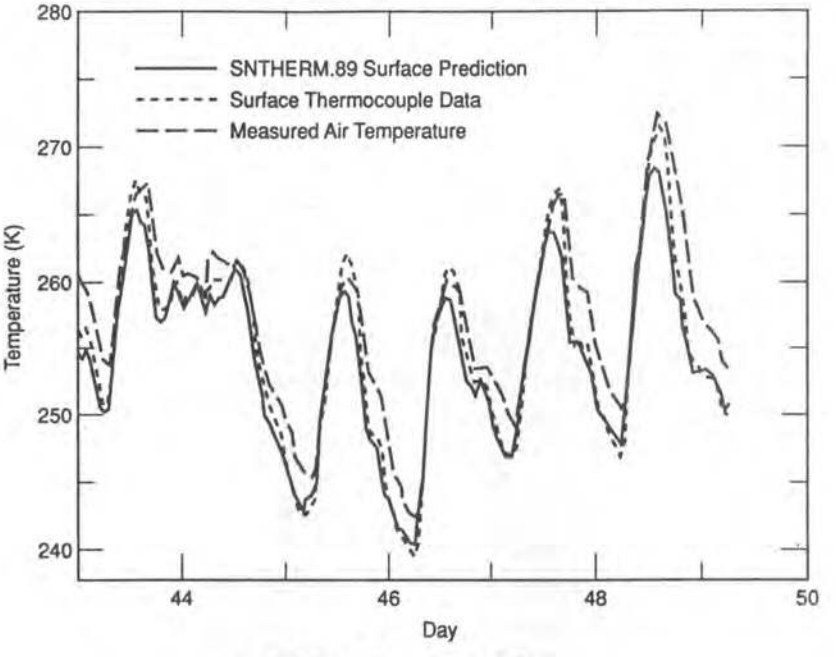

b. 12–18 February 1987.

Figure 11. Comparison of predicted vs measured surface temperatures for snow at Hanover, New Hampshire.

compares measured snow surface temperatures at the Hanover site with predictions from SNTHERM.89 for the period of 5–18 February 1987. The surface temperature of snow is highly correlated to air temperature (indicated by the dotted line in the graphs). In general it warms towards the air temperature during the day and drops below by several degrees at night due to radiative cooling. Subsurface profiles also showed close agreement between measured and predicted values, except during windy periods, when the curvature of the profiles indicated wind penetration within the upper 10 cm of the snow cover. It is yet to be determined how much of this effect was the result of wind-flow channeling by the thermocouple support, and how much would occur naturally in an undisturbed snow cover.

The supporting algorithms for snow compaction, grain growth, snow accumulation, freeze–thaw cycles and meltwater infiltration have been tested on the data set of 5–18 February 1987, which contained three periods of melt and two minor snowfall events. Preliminary testing has been done on subsequent data sets with periods of more active water flow. Water appears to be drawn down into the pack at a faster rate than predicted by theory, which may be corrected by including the capillary term or by using a lower value for the residual saturation. The model has been tested for the bare soil case but has not been verified with measurements. A more complete analysis of model performance is anticipated in conjunction with the extended version of the model, SNTHERM2.

CONCLUSIONS

An interim stage in the ongoing development for a model of the heat and mass flow through snow has been presented as technical documentation for the computer program SNTHERM.89. The program is coded in standard FORTRAN-77, and its implementation is further described in a preliminary user's guide (Jordan 1990). The expanded model version, SNTHERM2, which should be available within the calendar year, will contain many of the improvements noted in the report, including a two-stream radiative transfer algorithm for computing albedo and solar absorption and an extended water flow algorithm capable of simulating flow through soil and through a heterogeneous snow cover containing ice lenses.

LITERATURE CITED

Albert, M. (1983) Computer models for two-dimensional transient heat conduction. USA Cold Regions Research and Engineering Laboratory, CRREL Report 83-12.

Anderson, E.A. (1976) A point energy and mass balance model of a snow cover. Office of Hydrology, National Weather Service, Silver Spring, Maryland, NOAA Technical Report NWS 19.

Andreas, E.L. and B. Murphy (1986) Bulk transfer coefficients for heat and momentum over leads and polynyas. *Journal of Physical Oceanography,* **16** (11): 1875–1883.

Andreas, E.L. (1987) A theory for the scalar roughness and the scalar transfer coefficients over snow and sea ice. *Boundary-Layer Meteorology,* **38:** 159–184.

Bohren, C. and B. Barkstrom (1974) Theory of the optical properties of snow. *Journal of Geophysical Research,* **79** (30): 4527–4535.

Brooks, R.H. and A.T. Corey (1964) Hydraulic properties of porous media. Hydrology Papers, Colorado State University, Fort Collins, Colorado.

Buck, A. (1981) New equations for computing vapor pressure and the enhancement factor. *Journal of Applied Meteorology,* **20** (12)**:** 1527–1532.

Colbeck, S.C. (1971) One-dimensional water flow through snow. USA Cold Regions Research and Engineering Laboratory, Research Report 296.

Colbeck, S.C. (1972) A theory of water percolation in snow. *Journal of Glaciology,* **11** (63): 369–385.

Colbeck, S.C. (1973) Theory of metamorphism of wet snow. USA Cold Regions Research and Engineering Laboratory, Research Report 313.

Colbeck, S.C. (1974a) On predicting water runoff from a snow cover. In *Advanced Concepts and Techniques in the Study of Snow and Ice Resources* (H.S. Santeford and J.L. Smith, ed.), Washington, D.C.: National Academy of Sciences, p. 55–66.

Colbeck, S.C. (1974b) The capillary effects on water percolation in homogeneous snow. *Journal of Glaciology*, **13** (67): 85–97.

Colbeck, S.C. (1976) An analysis of water flow in dry snow. *Water Resources Research*, **12** (3): 523–527.

Colbeck, S.C. (1979) Water flow through heterogeneous snow. *Cold Regions Science and Technology*, **1:** 37–45.

Colbeck, S.C. (1982) An overview of seasonal snow metamorphism. *Reviews of Geophysics and Space Physics*, **20** (1): 45–61.

Colbeck, S.C. (1983a) Theory of metamorphism of dry snow. *Journal of Geophysical Research*, **88** (C9): 5475–5482.

Colbeck, S.C. (1983b) Ice crystal morphology and growth rates at low supersaturations and high temperatures. *Journal of Applied Physics*, **54** (5): 2677–2682.

Colbeck, S.C. (1986) Statistics of coarsening in water-saturated snow. *Acta Metallurgica*, **34** (3): 347–352.

Colbeck, S.C. (1987) A review of the metamorphism and classification of seasonal snow cover crystals. *Avalanche Formation, Movement and Effects, Proceedings of the Davos Symposium*, September, 1986.

Colbeck, S. C. (1989) Air movement in snow due to windpumping. *Journal of Glaciology*, **35** (120): 209–213.

Colbeck, S.C. and E.A. Anderson (1982) The permeability of a melting snow cover. *Water Resources Research*, **18** (4): 904–908.

Corey, A.T. (1977) *Mechanics of Heterogeneous Fluids in Porous Media*. Fort Collins, Colorado: Water Resources Publications.

deQuervain, M.R. (1963) On the metamorphism of snow. In *Ice and Snow* (W. D. Kingery, ed.), Cambridge, Mass.: M. I. T. Press.

Dunne, T., A.G. Price and S.C. Colbeck (1976) The generation of runoff from subarctic snowpacks. *Water Resources Research*, **12** (4): 677–685.

Farouki, O.T. (1981) Thermal properties of soils. USA Cold Regions Research and Engineering Laboratory, CRREL Monograph 81-1.

Gow, A.J. (1969) On the rates of grains and crystals in South Polar firn. *Journal of Glaciology*, **8**: 241–252.

Gray, D.M. (1979) Snow accumulation and distribution. In *Proceedings: Modeling of Snow Cover Runoff* (S.C. Colbeck and M. Ray, ed.). USA Cold Regions Research and Engineering Laboratory, Special Report 79-36, p. 3–33.

Gubler, H. (1985) Model of dry snow metamorphism by interparticle vapor flux. *Journal of Geophysical Research*, **90** (C8).

Gunn, K.L.S. (1965) Measurements on new-fallen snow. McGill University, Montreal, Stormy Weather Group Scientific Report MW-44.

Guryanov, I.E. (1985) Thermal-physical characteristics of frozen, thawing and unfrozen grounds. *Fourth International Symposium on Ground Freezing*, Sapporo, Japan, p. 225–230.

Hodges, D.B., G.J. Higgins, P.F. Hilton, R.E. Hood, R. Shapiro, C.N. Touart and R.F. Wachtmann (1983) Final tactical decision aid (FTDA) for infrared (8-12 μm) systems—Technical background. Systems and Applied Sciences Corporation, Scientific Report No. 5. Air Force Geophysics Laboratory Report AFGL-TR-83-0022.

Hicks, B.B. and H.C. Martin (1972) Atmospheric turbulent fluxes over snow. *Boundary-Layer Meteorology*, **2:** 496–502.

Idso, S.B. (1981) A set of equations for full spectrum and 8–14 μm and 10.5–12.5 μm thermal radiation from cloudless skies. *Water Resources Research*, **17:** 295–304.

Johansen, O. (1975) Thermal conductivity of soils. Ph.D. thesis, Trondheim, Norway. USA Cold Regions Research and Engineering Laboratory, CRREL Draft Translation 637, 1977.

Jordan, R., H. O'Brien and R.E. Bates (1986) Thermal measurements in snow. In *Snow Symposium V*, vol. 1, USA Cold Regions Research and Engineering Laboratory, Special Report 86-15, p. 183–193.

Jordan, R., H. O'Brien and M.R. Albert (1989) Snow as a thermal background: Preliminary results from the 1987 field test. USA Cold Regions Research and Engineering Laboratory, Special Report 89-7, p. 5–24.

Jordan, R. (1990) User's guide for CRREL one-dimensional snow temperature model. Available upon request from the author, CRREL.

Jordan, R. (In prep.) One-dimensional temperature model for a snow cover and frozen ground.

Kattelmann, R. (1986) Measurements of snow layer water retention. *Proceedings of the Cold Regions Hydrology Symposium, American Water Resources Association* (D. L. Kane, ed.), p. 377–386.

Kojima, K. (1967) Densification of seasonal snow covers. *Physics of Ice and Snow, Proceedings of an International Conference on Low Temperature Science, Institute of Low Temperature Science, Hokkaido University, Sapporo, Japan*, Vol. 1, Part 2, p. 929–952.

Kondo, J. and H. Yamazawa (1986) Bulk transfer coefficient over a snow surface. *Boundary-Layer Meteorology*, **34:** 125–135.

Lunardini, V.J. (1988) Heat conduction with freezing or thawing. USA Cold Regions Research and Engineering Laboratory, Monograph 88-1.

Marsh, P. and M.K. Woo (1984a) Wetting front advance and freezing of meltwater within a snow cover. 1. Observations in the Canadian Arctic. *Water Resources Research*, **20** (12): 1853–1864.

Marsh, P. and M.K. Woo (1984b) Wetting front advance and freezing of meltwater within an Arctic snow cover. 2. A simulation model. *Water Resources Research*, **20** (12): 1865–1874.

Mellor, M. (1964) Properties of snow. USA Cold Regions Research and Engineering Laboratory, Cold Regions Science and Engineering Monograph III-A1.

Mellor, M. (1977) Engineering properties of snow. *Journal of Glaciology*, **19** (81): 15–66.

Morland, L.W., R.J. Kelly and E.M. Morris (1990) A mixture theory for a phase-changing snowpack. *Cold Regions Science and Technology*, **17:** 271–285.

Morris, E.M and J. Godfrey (1979) The European Hydrologic System Snow Routine. In *Proceedings: Modeling of Snow Cover Runoff* (S. C. Colbeck and M. Ray, ed.). USA Cold Regions Research and Engineering Laboratory, Special Report 79-36, p. 269–278.

Morris, E.M. (1987) Modeling of water flow through snowpacks. In *Seasonal Snow Covers: Physics, Chemistry, Hydrology* (Jones and Orville-Thomas, ed.), p. 179–208.

Patankar, S.V. (1980) *Numerical Heat Transfer and Fluid Flow*. New York: Hemisphere Publishing.

Shimizu, H. (1970) Air permeability of deposited snow. Institute of Low Temperature Science, Sapporo, Japan, Contribution No. 1053. English Translation.

Shapiro, R. (1982) Solar radiative flux calculations from standard surface meteorological observations. Systems and Applied Sciences Corporation, Riverdale, Maryland, Scientific Report No. 1. Under contract to Air Force Geophysics Laboratory, Report AFGL-TR-82-0039.

Shapiro, R. (1987) A simple model for the calculation of the flux of direct and diffuse solar radiation through the atmosphere. ST Systems Corporation, Lexington, Massachusetts, Scientific Report No. 35. Under contract to Air Force Geophysics Laboratory, Report AFGL-TR-87-0200.

Siegal, R. and J.R. Howell (1972) *Thermal Radiation Heat Transfer*. New York: McGraw-Hill.

Smith, G.D. (1978) *Numerical Solution of Partial Differential Equations: Finite Difference Methods*. Oxford: Clarendon Press.

Stephenson, P.J. (1967) Some considerations of snow metamorphism in the Arctic ice sheet in the light of ice crystal studies. *Physics of Ice and Snow, Proceedings of an International Conference on Low Temperature Science, Institute of Low Temperature Science, Hokkaido University, Sapporo, Japan*, p. 725–740.

Tice, A.R., D.M. Anderson and A. Banin (1976) The prediction of unfrozen water contents in frozen soil from liquid limit determinations. USA Cold Regions Research and Engineering Laboratory, CRREL Report 76-8.

Wakahama, G. (1965) Metamorphisms of wet snow. *Low Temperature Science*, Series A (23): 51–66.

Warren, S.G. (1982) Optical properties of snow. *Reviews of Geophysics and Space Physics*, **20** (1): 67–89.

Wiscombe, W.J. and S.G. Warren (1980) A model for the spectral albedo of snow. I: Pure snow. *Journal of the Atmospheric Sciences*, **37** (12): 2712–2733.

Yen, Y.C. (1962) Effective thermal conductivity of ventilated snow. *Journal of Geophysical Research*, **67** (3): 1091–1098.

Yen, Y.C. (1963) Heat transfer by vapor transfer in ventilated snow. *Journal of Geophysical Research*, **68** (4): 1093–1101.

Yoshida, Z. (1950) Heat transfer by water vapor in a snow cover. *Low Temperature Science*, **5**: 93–100.

Yoshida, Z. (1963) Physical properties of snow. In *Ice and Snow* (W.D. Kingery, ed.). Cambridge, Mass.: M.I.T. Press.

REPORT DOCUMENTATION PAGE

Form Approved
OMB No. 0704-0188

1. AGENCY USE ONLY (Leave blank)	2. REPORT DATE	3. REPORT TYPE AND DATES COVERED
	October 1991	

4. TITLE AND SUBTITLE

A One-Dimensional Temperature Model For a Snow Cover: Technical Documentation for SNTHERM.89

5. FUNDING NUMBERS

PE: 6.11.02A
PR: 4A161102AT24
TA: FS
WU: 010

6. AUTHORS

Rachel Jordan

7. PERFORMING ORGANIZATION NAME(S) AND ADDRESS(ES)

U.S. Army Cold Regions Research and Engineering Laboratory
72 Lyme Road
Hanover, New Hampshire 03755-1290

8. PERFORMING ORGANIZATION REPORT NUMBER

Special Report 91-16

9. SPONSORING/MONITORING AGENCY NAME(S) AND ADDRESS(ES)

Office of the Chief of Engineers
Washington, D.C. 20314-1000

10. SPONSORING/MONITORING AGENCY REPORT NUMBER

11. SUPPLEMENTARY NOTES

12a. DISTRIBUTION/AVAILABILITY STATEMENT

Approved for public release; distribution is unlimited.

Available from NTIS, Springfield, Virginia 22161

12b. DISTRIBUTION CODE

13. ABSTRACT (*Maximum 200 words*)

This report provides technical documentation for the computer code SNTHERM.89, which is a one-dimensional mass and energy balance model of snow and frozen soil. The model is structured using a simplified mixture theory and addresses coupled mass and heat flow, phase change and snow metamorphism. The underlying theory and numerical equations are presented. Included are detailed descriptions of the computation of the energy fluxes at the air/snow interface and of optional routines for estimating short- and long-wave radiation on horizontal and sloped surfaces.

14. SUBJECT TERMS

Computer models | Mathematical models | Snow | Snow covers

15. NUMBER OF PAGES
64

16. PRICE CODE

17. SECURITY CLASSIFICATION OF REPORT	18. SECURITY CLASSIFICATION OF THIS PAGE	19. SECURITY CLASSIFICATION OF ABSTRACT	20. LIMITATION OF ABSTRACT
UNCLASSIFIED	UNCLASSIFIED	UNCLASSIFIED	UL

NSN 7540-01-280-5500

Standard Form 298 (Rev. 2-89)
Prescribed by ANSI Std. Z39-18
298-102